AGU PUBLICATIONS

Global Biogeochemical Cycles

RESEARCH ARTICLE
10.1002/2015GB005332

Key Points:
- River export of DOC has increased to the Gulf of Maine (GoM) over the last 80 years
- The GoM has yellowed in the last century with increased colored dissolved organic carbon (CDOM)
- Optical scattering from unidentified submicron particles is elevated in CDOM-rich river water

Supporting Information:
- Text S1, Table S1, and Figures S1–S8

Correspondence to:
W. Balch,
bbalch@bigelow.org

Citation:
Balch, W., T. Huntington, G. Aiken, D. Drapeau, B. Bowler, L. Lubelczyk, and K. Butler (2016), Toward a quantitative and empirical dissolved organic carbon budget for the Gulf of Maine, a semi-enclosed shelf sea, *Global Biogeochem. Cycles*, *30*, 268–292, doi:10.1002/2015GB005332.

Received 13 NOV 2015
Accepted 18 JAN 2016
Accepted article online 20 JAN 2016
Published online 20 FEB 2016

Toward a quantitative and empirical dissolved organic carbon budget for the Gulf of Maine, a semienclosed shelf sea

William Balch[1], Thomas Huntington[2], George Aiken[3], David Drapeau[1], Bruce Bowler[1], Laura Lubelczyk[1], and Kenna Butler[3]

[1]Bigelow Laboratory for Ocean Sciences, East Boothbay, Maine, USA, [2]U.S. Geological Survey, Augusta, Maine, USA, [3]U.S. Geological Survey, Boulder, Colorado, USA

Abstract A time series of organic carbon export from Gulf of Maine (GoM) watersheds was compared to a time series of biological, chemical, bio-optical, and hydrographic properties, measured across the GoM between Yarmouth, NS, Canada, and Portland, ME, U.S. Optical proxies were used to quantify the dissolved organic carbon (DOC) and particulate organic carbon in the GoM. The Load Estimator regression model applied to river discharge data demonstrated that riverine DOC export (and its decadal variance) has increased over the last 80 years. Several extraordinarily wet years (2006–2010) resulted in a massive pulse of chromophoric dissolved organic matter (CDOM; proxy for DOC) into the western GoM along with unidentified optically scattering material (<0.2 μm diameter). A survey of DOC in the GoM and Scotian Shelf showed the strong influence of the Gulf of Saint Lawrence on the DOC that enters the GoM. A deep plume of CDOM-rich water was observed near the coast of Maine which decreased in concentration eastward. The Forel-Ule color scale was derived and compared to the same measurements made in 1912–1913 by Henry Bigelow. Results show that the GoM has yellowed in the last century, particularly in the region of the extension of the Eastern Maine Coastal Current. Time lags between DOC discharge and its appearance in the GoM increased with distance from the river mouths. Algae were also a significant source of DOC but not CDOM. Gulf-wide algal primary production has decreased. Increases in precipitation and DOC discharge to the GoM are predicted over the next century.

1. Introduction: Global Fluxes of Dissolved Organic Carbon and Chromophoric Dissolved Organic Matter From Land to Sea

The flux of carbon from land to sea is a critical part of the global carbon cycle that has been studied for decades [*Boysen-Jensen*, 1914; *Waksman*, 1933]. Terrestrially dissolved organic carbon in rivers can be optically active and influence the color of seawater, particularly near coasts [*Andrew et al.*, 2013; *Blough et al.*, 1993; *Bricaud et al.*, 1981]. Referred to as "chromophoric dissolved organic matter" (CDOM), this material originates primarily from aromatic molecules produced by vascular plants [*Bricaud et al.*, 1981; *Hedges et al.*, 1997]. *Forel* [1890] and *Ule* [1892] devised a color comparator scale (henceforth referred to as the Forel-Ule (FU) color scale) for describing the variability in the reflectance spectrum associated with the transitions from ocean to CDOM-laden river waters. Observations of the sea using these color scales offers perhaps the longest record of ocean color available [*Wernand and Van Der Woerd*, 2010].

The estimated 0.4 Gt of terrestrial, allocthonous organic carbon supplied by rivers to the ocean annually [*Hedges et al.*, 1997] represents ~1% of the annual terrestrial carbon production [*Siegenthaler and Sarmiento*, 1993]. The relationship of dissolved organic carbon (DOC) concentration in rivers to its constituent CDOM absorption coefficient is well known [*Del Vecchio and Blough*, 2004; *Vodacek et al.*, 1997]. However, as one moves into the open ocean, relationships break down [*Siegel et al.*, 2002], likely related to the fact that rivers are no longer the primary source of DOC (and microflora become the primary source), plus CDOM photooxidation lowers the CDOM absorbance signal:noise for use as a DOC proxy [*Andrew et al.*, 2013; *DeGrandpre et al.*, 1996]. Satellite algorithms to predict CDOM absorption from satellite-based ocean color have been derived previously, and they show the apparent photooxidation of CDOM away from the Delaware River, midway out from the continental shelf to the continental slope region [*Mannino et al.*, 2008]. It is important to note that phytoplankton excrete 10–85% of their fixed carbon as labile DOC [*Carlson et al.*, 1998; *Mague et al.*, 1980]; thus, they can potentially represent a major source of DOC in waters not affected by rivers.

The spectral slope of CDOM and its variability has been described in many studies [*Bricaud et al*., 1981; *Green and Blough*, 1994; *Mannino et al*., 2008; *Roesler and Perry*, 1989; *Stedmon and Markager*, 2001]. In coastal waters, knowledge of the CDOM absorption per unit DOC (aka carbon-specific absorptive cross section of CDOM or specific UV absorbance; m^2 (g DOC)$^{-1}$) and measurements of the blue absorption of filtered sea water can allow the optical estimation of DOC concentrations. Further, because blue-absorbing CDOM can be observed from space, it should be possible to estimate surface DOC using information on absorption at the blue end of the spectrum and especially when using the spectral slope of this absorption [*Fichot and Benner*, 2012].

The Gulf of Maine (GoM) is an excellent system to study the influences of terrestrial sources of organic matter on marine waters and to address the use of space-based measurements to understand the distribution and fate of this material in the ocean. In addition, to open ocean waters, organic matter in the GoM is strongly influenced by the discharge of rivers in Maine and Maritime provinces of Canada that transport large quantities of CDOM-rich dissolved organic matter (DOM). Waters from the St. Lawrence River, the second largest river in North America, also deliver considerable CDOM-rich DOC into the Gulf of St. Lawrence, the waters of which can mix with the Labrador Current and be carried along the Scotian Shelf into the GoM [*Smith et al*., 2001].

There is evidence that patterns of DOC discharge into the sea are changing with changes in the hydrological cycle. Climate change has been associated with an intensification of the hydrological cycle during the 20th century, showing increased evaporation and precipitation [*Huntington*, 2006]. Greater variance in the hydrological cycle is predicted in the 21st century [*Seager et al*., 2012]. Increases in evaporation, precipitation, and runoff have also been observed over the northeastern U.S. [*Hayhoe et al*., 2007; *Huntington and Billmire*, 2014] and the St Lawrence River [*Walter et al*., 2004]. Such increases have been hypothesized to change the mobilization of carbon from the terrestrial realm and transport it to the sea [*Tranvik and Jansson*, 2002]. The variance of precipitation at some stations in the Gulf of Maine (GoM) watershed has increased over the last century, and large amounts of CDOM have been carried into the gulf as a result [*Balch et al*., 2012]. Similarly, *Sun et al*. [2012] found increasing variance in precipitation over the GoM watershed for the period 1940 to 2009.

There is a strong need to quantify the actual amount of organic matter moved to the GoM during these heavy precipitation events. From a measurement standpoint, optical proxies will be the best way to do this, where CDOM fluorescence will provide information on DOC concentration and particle backscattering can provide information on particulate organic carbon (POC) concentration. In this paper, we summarize 15 years of data from a coastal ocean time series across the GoM, on the distribution of dissolved and particulate organic carbon. We then relate this to an annual budget of river-produced, allochthonous organic carbon and phytoplankton-produced, autochthonous organic carbon in the GoM. Finally, using climate forecasting approaches, we predict future changes in CDOM and DOC in the GoM associated with river discharge.

2. Site Description

2.1. Gulf of Maine

The Gulf of Maine (GoM) is a productive continental shelf sea off the NE coast of the U.S. with a maximum water depth of ~300 m. The combined area of the Gulf of Maine and Georges Bank is about 132,700 km^2. It receives surface inflows of Scotian Shelf water (SS), some of which originates from the St. Lawrence Estuary. Deep intrusions of North Atlantic slope water enter the gulf through the Northeast Channel over a 230 m deep sill. Pulses of seawater periodically flow in through the Northeast Channel, over time scales of days to weeks, containing both warm North Atlantic slope water and cold Labrador slope water, with average transport of ~$262(\pm 58) \times 10^3$ m^3 s^{-1} [*Ramp et al*., 1985]. These inflows carry ~82% of the annual nitrogen influx into the gulf [*Townsend*, 1998].

2.2. Gulf of Maine Watershed

The GoM watershed covers an area of about 179,000 km^2 that includes 25 major river basins and 11 minor coastal drainage areas [*Thompson*, 2010]. The total discharge into the GoM is estimated to be ~3000 m^3 s^{-1} [*Meade and Emery*, 1971]. Fourteen watersheds contribute about half of the freshwater influx. The St. John River is the largest river flowing into the GoM, draining an area of about 55,000 km^2, and has an

average daily discharge of ~990 $m^3 s^{-1}$ at its mouth. The Penobscot River, ME, is the second largest river in New England, draining a 20,109 km^2 watershed with an average discharge of ~341 $m^3 s^{-1}$, peaking in March–April with a second peak in November–December. DOC is the dominant form of carbon discharged in all the watersheds. These watersheds consist of forest land (~89%) [*Griffith and Alerich*, 1996], lakes, swamps and ponds > 0.4 ha (5%), and agriculture (4%). About a quarter of the land area in Maine is palustrine wetland, and 40% of this is scrub/shrub or emergent vegetation, while the remaining 60% is forested. Ninety percent of the organic carbon transported via Maine and Canadian Maritime rivers is in the form of DOC [*Wetzel*, 1975], at typical concentrations of 4 to 15 mg C L^{-1}. Regardless of river discharge rate, riverine DOC concentrations are lowest in winter and spring, greater in summer, and greatest in fall (during high flow periods) (see also *Cronan et al.* [1999] and *Huntington and Aiken* [2013]). The CDOM supplied by these 25 watersheds can dominate the blue absorption in the GoM such that it far outweighs the absorption of phytoplankton in coastal waters, particularly at salinities <30 [*Balch et al.*, 2012; *Balch et al.*, 2004; *Yentsch and Phinney*, 1997].

2.3. Gulf of St. Lawrence Watershed

Another watershed with major impact on the coastal waters of NE North America and the Gulf of Maine is the St. Lawrence River. This 3058 km long river begins above Lake Ontario and drains the Great Lakes with a total watershed area of 1,030,000 km^2, has average discharge rates of 413 $km^3 yr^{-1}$ (13,096 $m^3 s^{-1}$) [*Pocklington and Tan*, 1987], and ultimately drains into the Gulf of Saint Lawrence (GoSL), arguably the largest estuary in the world. DOC concentrations in the St. Lawrence River are 2.5–5 mg C L^{-1} ([*Pocklington and Tan*, 1987] USGS data from Cornwall, Ontario), half the concentrations found in the Penobscot River (see above), possibly due to a much larger fraction of the watershed being in agriculture and large lakes. The bulk DOC in the St. Lawrence River is isotopically young, and its source is mainly recent organic matter from the watershed [*Butman et al.*, 2012; *Helie and Hillaire-Marcel*, 2006]. Downstream, several large rivers originating from the Canadian Shield drain into the GoSL from watersheds dominated by boreal forests and peatlands with elevated DOC concentration (>5 mg C L^{-1}) [*Hudon et al.*, 1996]. Three of those rivers (Saguenay, Manicouagan, and Aux-Outardes) have an average daily discharge of ~3100 $m^3 s^{-1}$, similar to the discharge into the GoM. By contrast, the runoff per unit area for the GoM watershed is ~1.5 times greater than the GoSL watershed and the DOC concentration is 2–2.5 times greater in the GoM watershed. Considering both the higher DOC concentration and the higher water yield (per unit area discharge) for Maine and Canadian Maritime rivers, the DOC inputs to the GoM are about 50% of those coming into the GoSL despite the differences in watershed area.

Water originating in the GoSL is thought to be traceable to the GoM about 8–12 months later [*Smith et al.*, 2001; *Sutcliffe et al.*, 1976]. It has been shown using $\delta^{18}O$ and salinity that SS and Labrador Sea water falls on a mixing line between the St Lawrence Estuary and the Gulf Stream, and DOC from the Gulf of St. Lawrence may be carried around Cape Breton, along the Scotian Shelf, and arrives in the Gulf of Maine [*Smith et al.*, 2001]. SS flows as a seasonally variable longshore coastal current, running southwestward along the eastern shore of Nova Scotia at 2–5 cm s^{-1}. It receives some upwelling circulation (0.5 cm s^{-1}) off Cape Sable [*Smith*, 1983].

3. Methods

The domain of this study is the watersheds that empty into the Gulf of Maine (GoM) as well as the Gulf of Maine and northward to the GoSL. We address these environments individually. A complete list of variables and abbreviations used in this work can be found in Tables 1 and 2.

3.1. Watershed Sampling

The watersheds addressed in this study are shown in Figure 1. Gauged watersheds in the study area include the Merrimack, Presumscot, Saco, Androscoggin, Kennebec, Sheepscot, Penobscot, Narraguagus, Dennys, St. Croix, and St. John Rivers. The ungauged watersheds (including in Maine, New Hampshire, Massachusetts, the lower St. John River, and areas in Nova Scotia draining to the Bay of Fundy) represent ~42% of the total water shed. A list of the rivers, sampling locations, USGS station IDs, drainage areas, periods of record for discharge and sampling for DOC concentration, number of samples, and rivers used for each analysis can be found in Table S1 in the supporting information.

Table 1. Definitions Used in This Work

Term	Units	Definition
a_{g412}	m^{-1}	Absorption of <0.2 mm particles at 412 nm (or whatever wavelength is designated)
a_{gp412}	m^{-1}	Total absorption for dissolved (<2 mm) and particulate (>2 mm particles) at 412 nm (or whatever wavelength is designated)
b_{bp532}	m^{-1}	Particle backscattering at 532 nm (or whatever wavelength is designated)
b_{g412}	m^{-1}	Dissolved (<0.2 mm-filtered) scattering at 412 nm
b_{gp412}	m^{-1}	Scattering of dissolved plus particulate materials at 412 nm (or whatever wavelength is designated)
b_{p532}	m^{-1}	Particle scattering at 532 nm (or whatever wavelength is designated)
c_{g412}	m^{-1}	Attenuation of dissolved (<2 mm-filtered) seawater at 412 nm (or whatever wavelength is designated)
nLw	$mW\ cm^{-2}\ \mu m^{-1}\ Sr^{-1}$	Normalized water-leaving radiance
S		Spectral slope of absorption between 275 and 295 nm
$SUVA_{254}$	$m^2\ (g\ DOC)^{-1}$	Specific UV absorption at 254 nm (or whatever wavelength is designated)

3.2. River Sampling

Continuous river discharge and discrete measurements of DOC concentration from major rivers flowing into the GoM have been maintained by the U.S. Geological Survey (Augusta, ME), with records from some parts of the watershed extending back over a century. Water quality data used in this study go back to 2004 for all rivers except for the Merrimack River where data were collected from 1998 to 2000 (Table S1). Sampling was conducted throughout the year and during periods of high discharge. River discharge was compiled from the USGS National Water Information System (NWIS) online database (http://dx.doi.org/10.5066/F7P55KJN) and New Brunswick Power Company. DOC data were assembled from the USGS National Water Information System database (NWIS, http://dx.doi.org/10.5066/F7P55KJN).

The Load Estimator (LOADEST) regression program was used to estimate DOC export using daily river discharge data plus paired, discrete instantaneous discharge data and DOC concentration data [*Runkel et al.*, 2004]. It predicts the variation in DOC concentration as a function of time of year and rate of discharge. Land surface characterization data were obtained from U.S. and Canadian Geographic Information Systems data bases including the Maine Geographic and Information System (http://megis.maine.gov/). A time series of DOC export was produced.

3.3. Chemical Analyses

Samples were immediately filtered and shipped on ice to the U.S. Geological Survey laboratories in Boulder, CO, where measurements were made for DOC concentration, specific UV absorption [*Weishaar et al.*, 2003], and the spectral slope (S) of absorption in the UV between 275 and 295 nm [*Green and Blough*, 1994]. Detailed methods

Table 2. Abbreviations Used in This Work

Abbreviations Used in Text	Full Name
AZMP	Atlantic Zone Monitoring Program
CDOM	Chromophoric dissolved organic matter
DOC	Dissolved organic carbon
DOM	Dissolved organic matter
EMCC	Eastern Maine Coastal Current
ExtEMCC	Extension of the Eastern Maine Coastal Current
FU	Forel-Ule color comparator scale
GNATS	Gulf of Maine North Atlantic Time Series
GoM	Gulf of Maine
GoSL	Gulf of St. Lawrence
IOP	Inherent optical property
JB	Jordan Basin
NERACOOS	Northeastern Regional Association of Coastal and Ocean Observing Systems
POC	Particulate organic carbon
SS	Scotian Shelf water
WB	Wilkinson Basin
WMCC	Western Maine Coastal Current

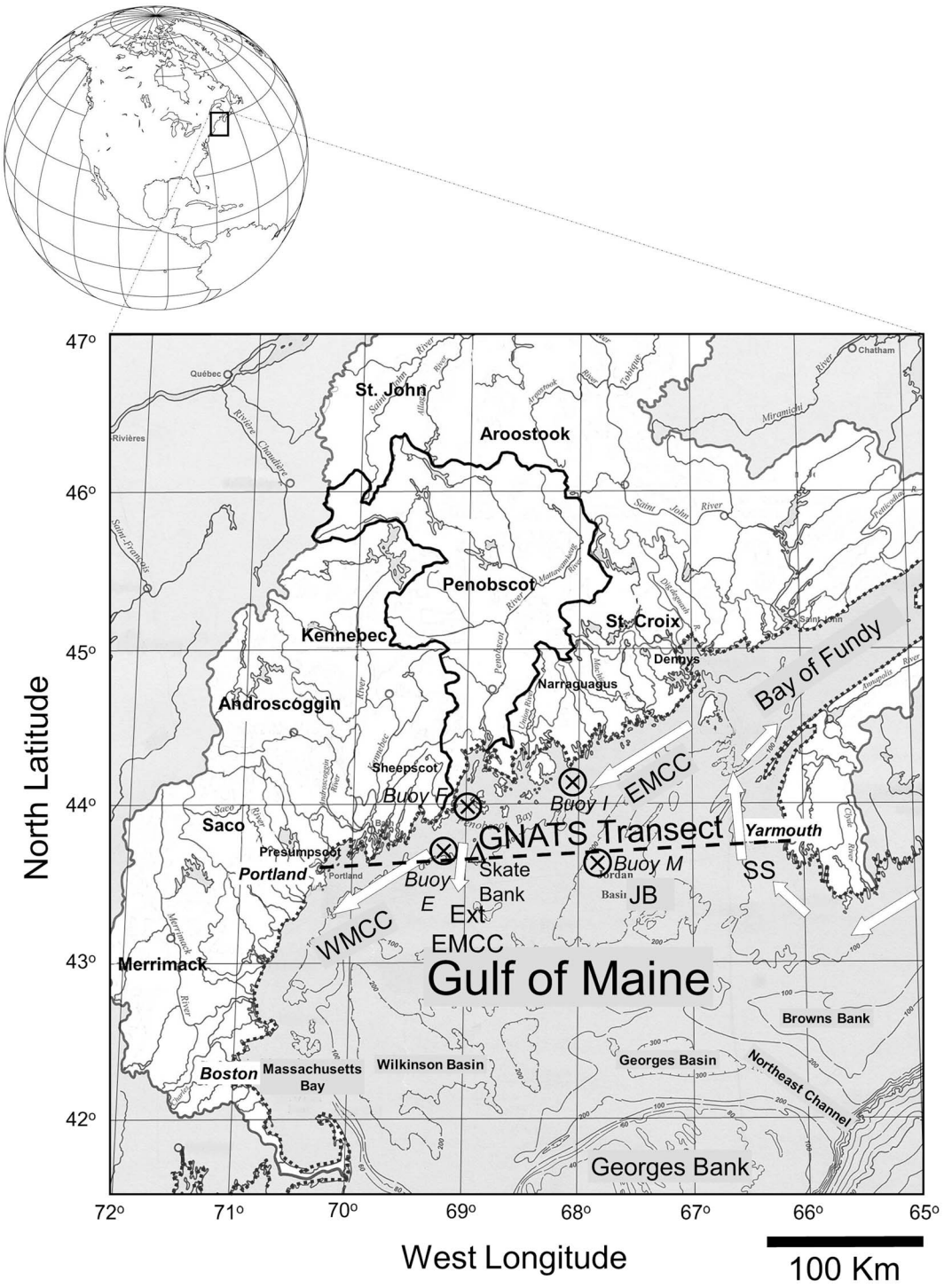

Figure 1. Map of study area showing the Gulf of Maine with bathymetry, plus terrestrial watersheds draining into it where there are DOC and runoff data to compute loads (the 11 gauged watersheds are the Merrimack, Saco, Presumpscot, Androscoggin, Kennebec, Sheepscot, Penobscot, St. Croix, St. John, Arrostook, Narraguagus, and Dennys, all shown with white shading) as well as watersheds that do not drain into it (lighter shade of gray). The Penobscot River watershed is specifically outlined with a solid black line. Coastline is demarcated with a dotted line. GNATS transect across the Gulf of Maine appears as a dashed line crossing between Portland, ME, and Yarmouth, NS. Water masses traversed during the transect are also indicated: Western Maine Coastal Current (WMCC), Eastern Maine Coastal Current (EMCC), Extension of the Eastern Maine Coastal Current (ExtEMCC), Jordan Basin (JB), and Scotian Shelf water (SS). Notable bathymetric features (banks and basins) are also designated. General mean surface current flow is shown with white arrows. Positions of Gulf of Maine NERACOOS buoys (E, F, I, and M) are shown.

of these chemical analyses are given in the supporting information. Note that while the UV bands provide the highest quality optical data for estimating DOC concentration (see section 4.2), the 412 nm band overlaps with bands on ocean color sensors (e.g., Moderate Resolution Imaging Spectroradiometer (MODIS) and Sea-viewing Wide Field-of-view Sensor). Using these data, we empirically derived the fraction of terrestrially derived DOC exported to the GoM, thereby integrating the multitude of biological, geological, and meteorological factors over the landscape, as well as changing export rates associated with climate change not included in models. A retrospective analysis of riverine DOC export was performed over the period between 2002 and 2013. The DOC flux data were extrapolated primarily using DOC field data from 2004 to 2013, however, for the Merrimack River data were collected between 1998 and 2000 (USGS NWIS http://dx.doi.org/10.5066/F7P55KJN).

3.4. Gulf of Maine Observations

The Gulf of Maine North Atlantic Time Series (GNATS) is a transect time series that runs between Portland, ME, and Yarmouth, NS (300 km transect; Figure 1). It was started in 1998, running on ships of opportunity such as ferries and other small research and commercial vessels.

3.4.1. GNATS Continuous Underway and Discrete Measurements

The GNATS underway system makes a suite of hydrographic, chemical, inherent optical properties (IOPs; e.g., absorption, scattering, attenuation, and backscattering), and apparent optical properties (above-water spectral upwelling radiance, sky radiance, and downwelling irradiance) measurements that are used to estimate the standing stock of POC and particulate inorganic carbon (PIC) and absorption of CDOM continuously as well as for ocean color sensor validation. A complete description of the system is described elsewhere [*Balch et al*., 2012; *Balch et al*., 2008]. More details for the continuous measurements are found in the supporting information. Every ~35 km across the GoM, nine discrete surface samples were taken from the underway sample stream. For each water sample, aliquots were subsampled for concentrations of PIC, POC, DOC, chlorophyll *a*, microscope counts of phytoplankton, ^{14}C-photosynthesis, and ^{14}C-calcification rate. From 2012 to 2014, the net rate of production of DOC was measured by retaining a subsample of the filtrate from the ^{14}C incubation, further filtering it through a 0.2 μm filter and measuring the quantity of ^{14}C activity following removal of all ^{14}C-dissolved inorganic carbon by acidification to a pH = 3 with 1 N H_2SO_4 [*Mague et al*., 1980]. What remained was the non-acid-labile ^{14}C-DOC that passed a 0.2 μm filter. This activity was quantified using liquid scintillation counting. (See supporting information for more details on above methods.)

3.4.2. Shipboard Above-Water Chromaticity

Colorimetry was used to examine changes in water color "chromaticity" along the GNATS transect for comparison to historical data [*Bigelow*, 1924]. The chromaticity of the water was defined based on the Commission Internationale de L'eclairage tristimulus, or color matching functions, which allow any spectral radiometric quantity to be converted to its equivalent colorimetric coordinates based on the sensitivity of the human eye [*Mobley*, 1994; *Wyszecki and Stiles*, 1982]. For converting radiance to the photometric quantity (luminance), equations 2.10a–c of *Mobley* [1994] were used, which incorporate the maximum luminous efficacy (K_m, the factor to convert radiometric power (watts) to photometric power (lumens)), the phototopic luminosity function (i.e., the 1931 tristimulus functions), and the observed spectral water-leaving radiance derived from Satlantic Surface Acquisition System (SAS) measurements, integrated over each waveband.

3.4.3. Autonomous Glider Measurements

A Slocum glider (Webb/Teledyne Research Corp.) was deployed 13 times from 2008 to 2014 along the GNATS transect. It was equipped with a WETLabs ECO-triplet (to measure the fluorescence of chlorophyll *a*, CDOM plus particle backscattering at 532 nm, b_{bp532}), conductivity-temperature-depth probe (to measure conductivity, temperature, and depth (pressure)), and Satlantic upwelling radiance sensor (seven wavelengths) and downwelling irradiance sensor (seven wavelengths). The glider took, on average, 23–24 days to cross the GoM and back. We used our shipboard optical and chemical measurements to calibrate the continuous glider measurements for converting CDOM to [DOC], b_{bp532} to [POC], and chlorophyll fluorescence to [chl *a*]. The glider was programmed to surface each 6 h in order to upload data via iridium satellite telemetry and verify position using GPS. Missions 2 and 8 (both eastbound and westbound sections), and 3 (westbound section only) were incomplete due to glider malfunctions; hence, the sections were incomplete and not included here. There were no glider deployments in 2011 due to a hiatus in the GNATS program.

3.4.4. Scotian Shelf Measurements

Water samples were taken from one Atlantic Zone Monitoring Program (AZMP) cruise, Canada from near Cabot Strait, north of Cape Breton, around the Scotian Shelf of Nova Scotia, in October 2012, to better

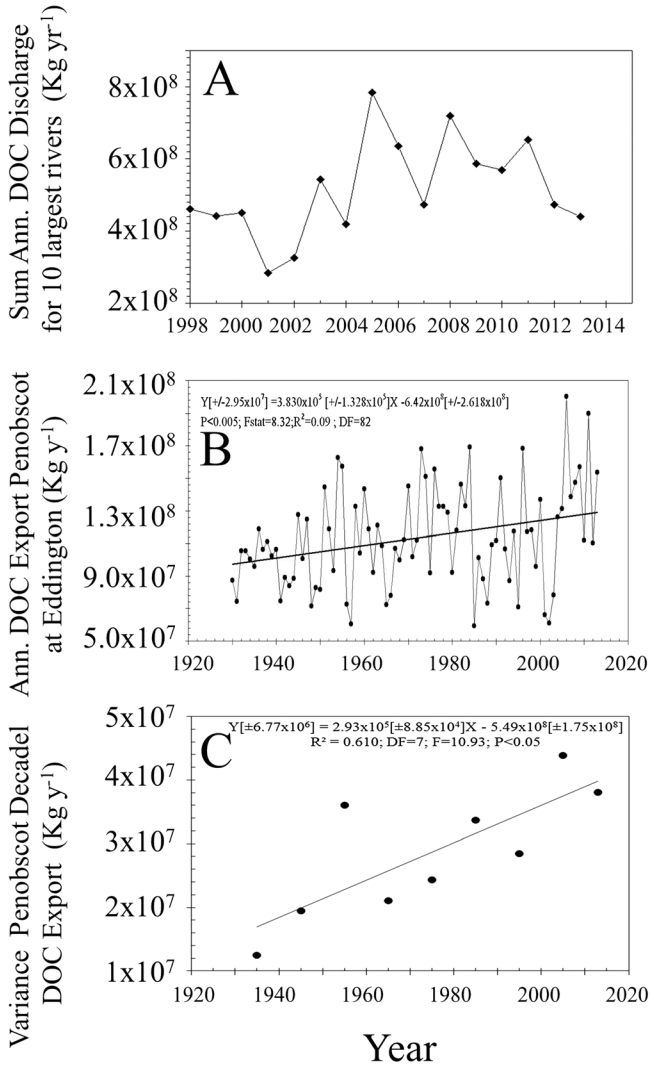

Figure 2. Time series of river discharge of DOC (kg DOC yr^{-1}) based on river discharge data and the LOADEST model. (a) Sum of 10 largest rivers emptying into the Gulf of Maine from 1998 to 2013. (b) Time series of DOC export for the Penobscot River between 1930 and 2013. (c) Time series of decadal variance in Penobscot DOC export, derived from data in Figure 2b. Linear, least squares fit and associated statistics given for statistically significant relationships in Figures 2b and 2c, with standard error terms for each fit coefficient shown in square brackets.

understand the DOC characteristics of the SS entering the GoM. Samples were immediately shipped on ice to the USGS (National Research Program, Boulder, CO) for DOC analyses as described above.

3.4.5. Satellite Derivation of DOC

SeaDAS software was used to process all MODIS ocean color data. The Generalized Inherent Optical Property (GIOP) algorithm [*Werdell et al.*, 2013] was implemented to estimate a_{g412} from spectral normalized water-leaving radiance (nLw). Then the best fit, empirically derived algorithm to convert a_{g412} to DOC (based on shipboard measurements) was applied.

3.5. Future Predictions of DOC Discharge

To predict future DOC discharge, we used climate projections for the northeastern U.S. from the United Kingdom Meteorological Office Hadley Centre (HadCM3) [*Gordon et al.*, 2000; *Pope et al.*, 2000] forced with the A1FI emission scenario [*Nakićenović*, 2000]. We used the Variable Infiltration Capacity (VIC) hydrologic model [*Liang et al.*, 1996] output developed for this region as described in *Hayhoe et al.* [2007]. Briefly, for the hydrological projections, a monthly atmosphere ocean coupled general circulation model was used. Temperature and precipitation fields were first statistically downscaled to daily values with a resolution of 1/8°. Downscaled temperature and precipitation were then used as input to the Variable Infiltration Capacity (VIC) land surface hydrological model, to calculate future changes in hydrology. More details about the climate projections performed here can be found elsewhere (T. Huntington et al., Climate change and dissolved organic carbon export to the Gulf of Maine, submitted to *Journal of Geophysical Research: Biogeosciences*, 2015).

4. Results

4.1. Discharge of DOC From Rivers Over the Last Century

LOADEST estimates for DOC discharge rates from the 10 largest gauged watersheds emptying into the GoM, for the period 1998–2013, are shown in Figure 2a. The total annual DOC discharge rates for these rivers varied by about a factor of 3 over the 16 years, from 2.75×10^8 to 8×10^8 kg yr^{-1}. The results showed an increasing trend during the period that GNATS has been run, although the least square linear fit was not significant (F test, $P > 0.05$). Longer trends in DOC export can only be tested using the longer data set from the Penobscot River, as measured at Eddington between 1930 and 2013 (Figure 2b). For the Penobscot over this

period, DOC discharge rates varied from ~5.5×10^7 to 2.0×10^8 kg DOC yr^{-1}. There was a significant (*F* test; $P < 0.005$) but low correlation ($r^2 = 0.09$) relationship between DOC discharge rate per year versus time, with a slope of 3.83×10^5 [$\pm 1.33 \times 10^5$] kg DOC yr^{-1} (=0.383 Gg yr^{-1}). This annual increase in DOC flux, averaged over the area of the Penobscot watershed (2.22×10^{10} m^2), represents an additional increase in watershed yield of 0.208 g DOC m^{-2} yr^{-1}.

4.2. Optical Proxies of DOC Concentration Based on CDOM

Based on the entire GNATS data set, the correlation between dissolved absorption, a_g, and DOC (mg C L^{-1}) improved at progressively shorter wavelengths from 412, 350, and 254 nm, with the coefficient of determination (r^2) increasing from 0.331, 0.624, and 0.670, respectively (Figures S1A–C). All correlations were significant based on the *F* test at $P < 0.001$. The standard error (SE) of the predicted DOC concentration based on the above relationships also improved when using progressively shorter wavelengths (±0.91, ±0.66, and ±0.61 mg C L^{-1}, respectively). The prediction of DOC concentration was improved further using the approach of *Fichot and Benner* [2011] in which both a_{g254} and the spectral slope between 275 and 295 nm were used. In this case, the SE of the DOC estimate in the GoM was ±0.45 mg C L^{-1} (Figure S1D; $r^2 = 0.81$; $P < 0.001$), about half of the SE if the prediction is based just on a_{g412}.

4.3. Spatial Variability of DOC and CDOM

The space-time variability of DOC in the GNATS transect showed a pulse of surface DOC concentration in the western third of the transect in the period 2006–2010 (Figure S2A). There also was enhanced DOC on the eastern side of the gulf in 2005–2007. After 2010, DOC concentrations dropped to levels seen before the 2006–2010 pulse. CDOM (dissolved absorption; a_{g412}) showed similar enhancement in the western side of the GoM with highest concentrations in 2006–2010 (Figures 3a and S2B). Total absorption at 412 nm (dissolved plus particulate; Figure S2C) showed similar spatial/temporal trends as for just a_{g412}, from 2006 to 2010 but with relatively more enhancement on the eastern side. POC concentrations (Figure S2D) were strongly enhanced in the western GoM during the early years of the program, which gave way to lower and more evenly distributed concentrations in 2006. Particulate backscattering at 532 nm (Figure S2E) roughly paralleled the patterns of a_{gp412} (Figure S2C) showing enhancement on the east and west sides of the GoM from 2006 to 2010. Dissolved total scattering at 412 nm (estimated as the difference, $c_{g412} - a_{g412}$; Figure S2F) showed a different pattern from backscattering, with values across the entire GoM from 2006 to 2010 elevated ~10 times.

Average CDOM absorption, measured with the ac-9, and binned by longitude, showed clear geographic variability across the GNATS transect, with highest absorption in the west (in near-shore waters of the Western Maine Coastal Current) and a lesser peak at the east end of the transect (in near-shore Scotian Shelf (SS) Water) (Figure 3). There also is a slightly enhanced double peak in absorption from 68.8 to 69.2°W longitude, the rough position of the extension of the Eastern Maine Coastal Current (ExtEMCC), which crosses through the GNATS transect. Lowest average CDOM absorption was observed from 66.7 to 68.2°W longitude in Jordan Basin (JB) waters. A similar pattern was observed for the sum of CDOM and particle detritus (a_{gp412}; Figure 3b).

Total scattering (*b*) of CDOM and particle detritus was estimated from the difference between attenuation (*c*) and absorption (*a*) at 412 nm. That is, $b_{g412} = c_{g412} - a_{g412}$ or $b_{pg412} = c_{pg412} - a_{pg412}$, where the subscript "g" denotes "gelbstoff" or water filtered through a 0.2 μm filter and subscript "p" denotes particulate material >0.2 μm diameter. Thus, the subscript "gp" refers to total, unfiltered seawater including both dissolved and particulate matter (Figure 4). Values of b_{g412} were higher in the western gulf in the same waters where a_{g412} was enhanced. Similarly, on the eastern end, b_{g412} showed a lesser but still significant increase in the SS (Figure 4a). There was a small increase in the mean b_{g412} associated with the crossing of the ExtEMCC, in the same location were a_{g412} also increased. Scattering of combined CDOM and particulate detritus (b_{pg412}) increased significantly at east and west ends of the transect, but on the eastern side in SS water, b_{pg412} values were close to those seen in the WMCC. At the boundary between SS and JB water (66.7°W), there was a small peak in both b_{g412} and b_{pg412} (Figure 4). Values of b_{g412} were significantly correlated to a_{g412} (as shown in Figure 3a) measured in the same geographic bins (see inset to Figure 4a).

Water samples from the Canadian Department of Fisheries and Oceans cruise (October, 2012) showed highest concentrations of DOC from near Cabot Strait, followed around the eastern side of Cape Breton and Nova

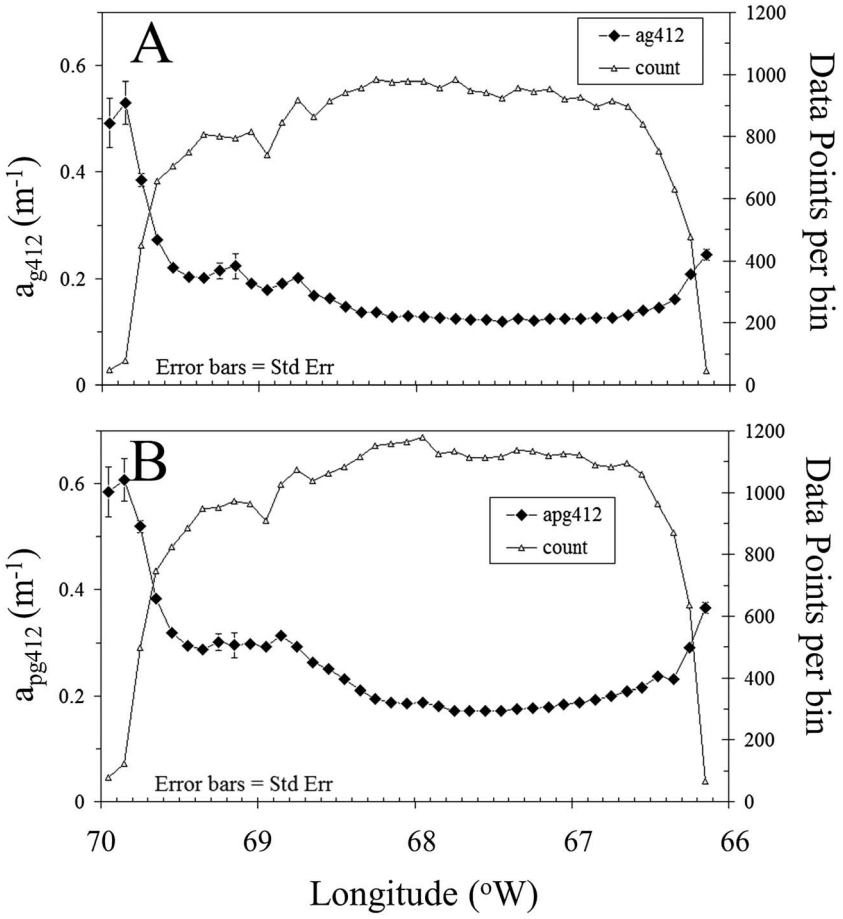

Figure 3. Absorption of chromophoric dissolved organic matter and detritus across the GNATS transect. (a) Average CDOM absorption, a_{g412}, plotted against longitude (solid diamonds). Error bars represent one standard error about the mean. Data binned in 0.1° longitude bins. Number of data points designated by open triangles (right *Y* axis). (b) Same as in Figure 3a except the total dissolved and particulate absorption at 412 nm (a_{gp412}) plotted against longitude (solid diamonds) and number of data points in each bin shown as open triangles.

Scotia. Lower concentrations were observed offshore than onshore. Coastal DOC concentrations decreased as waters flowed to the southwest before entering the GoM (Figure 5a). There was a moderate, but significant, inverse correlation between the DOC concentration and salinity. Moreover, the specific UV absorption at 254 nm ($SUVA_{254}$; m^2 (g DOC)$^{-1}$; see supporting information) also declined from low- to high-salinity waters (Figure 5b).

4.4. Satellite-Derived CDOM Concentrations

MODIS Aqua data of the GoM and GoSL were used with the GIOP algorithm to estimate a_{g412}. We then applied the best fit relation between ship-derived a_{g412} and ship-derived DOC concentrations (Figure S1A) to derive a GoM-specific algorithm to estimate surface DOC concentrations based on satellite-derived optical data. Using a MODIS image from fall 2005 (which followed a major precipitation event), DOC concentrations were estimated in both the GoM and GoSL (Figure 6). As with the ship data from October 2012, highest concentrations of DOC were observed near the Cabot Straits, as well as around Prince Edward Island and the NE coast of New Brunswick/Gaspe Peninsula, and southwest along the eastern coast of Nova Scotia into the GoM. Concentrations again increased within the EMCC and in WMCC waters, with low-level CDOM enhancement seen in SS waters. The ExtEMCC was visible as a tongue of elevated DOC concentration extending offshore and bifurcating with part extending into JB water and part into Wilkinson Basin (WB) water further to the south. DOC loss from the GoM could be visualized extending south and east from Georges Bank (Figure 6).

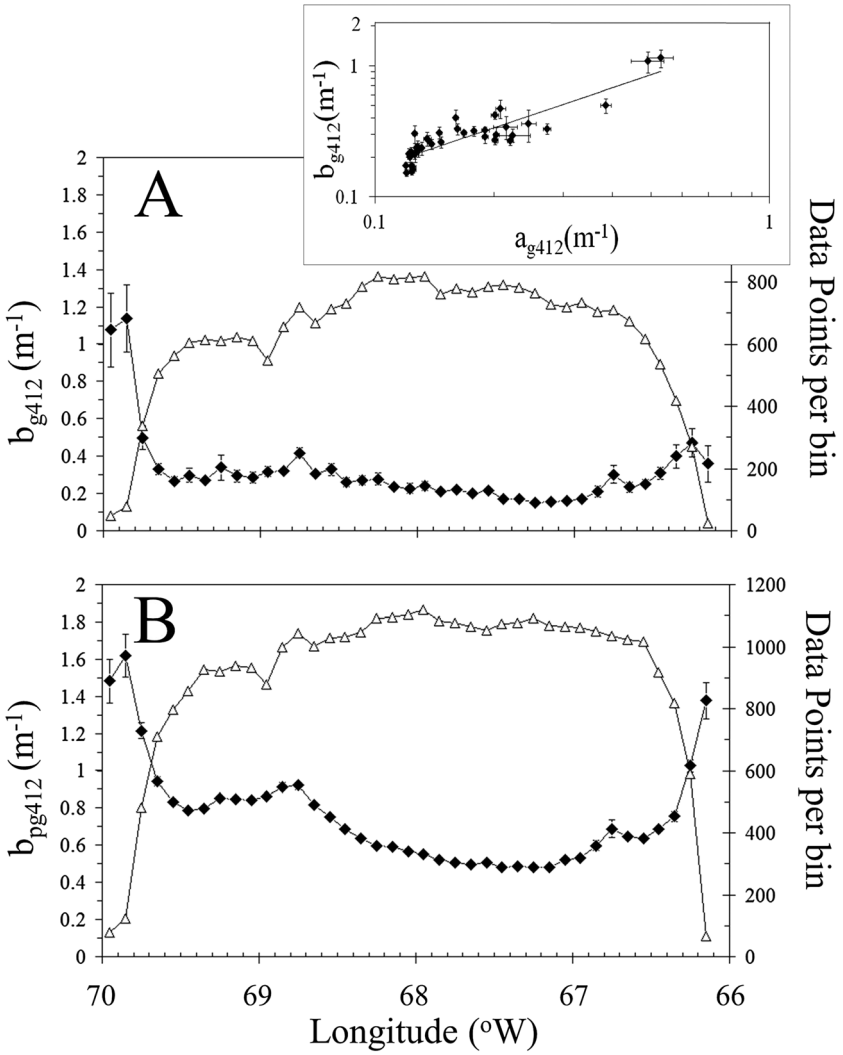

Figure 4. Optical scattering of chromophoric dissolved organic matter and detritus in surface waters across the GNATS transect. (a) Average CDOM scattering, b_{g412}, plotted against longitude (solid diamonds). Number of data points designated by open triangles (right *Y* axis). Inset shows b_{g412} plotted against a_{g412} from Figure 3a, plotted on log axes. Power fit to inset data (b_{g412} [±0.088] = 1.7163[±0.272] $a_{g412}^{1.0127[\pm 0.087]}$; $r^2 = 0.787$; d.f. = 37; $P < 0.001$), where values in square brackets are standard errors to fit coefficients. Error bars for panel and inset represent one standard error about the mean. (b) Same as in Figure 4a except the total dissolved and particulate scattering at 412 nm (b_{pg412}) plotted against longitude (solid diamonds) and number of data points in each bin shown as open triangles. Data in panels and inset binned in 0.1° longitude bins.

4.5. Glider-Derived DOC and POC Distributions

The glider provided unique abilities to estimate vertical sections of DOC and POC along the GNATS transect. The DOC sections (e.g., Figure 7a) were estimated from the optical proxy between CDOM fluorescence and measured DOC (mg C L^{-1}) for GoM GNATS samples. The mean relationship was statistically significant despite a low coefficient of correlation (DOC[±0.225] = 0.0395[±0.0158]cdom fluoresence + 1.066[±0.052]; $r^2 = 0.115$; d.f. = 48; $F = 6.23$; $P <= 0.05$). As expected from the satellite view (Figure 6), the DOC vertical section showed highest levels (1.2 mg L^{-1}) in the western GoM in the WMCC and ExtEMCC extending downward up to 100 m. DOC concentrations decreased further to the east, also as suggested by the satellite image (Figure 6). Surface concentrations of DOC in the top 10 m decreased to about 1.1 mg L^{-1} at about 69°W and from 68.4 to 67.3°W. The glider could only sample to 180 m, so there is no information on deeper DOC distributions in this study.

Vertical sections of POC concentration were estimated from the least squares power function derived from all GNATS ship measurements for b_{bp531} (m^{-1}) and POC concentration (μg C L^{-1}; logPOC[±0.201] = 0.377 [±0.023] × log b_{bp532};+3.208[±0.057]; $r^2 = 0.193$; d.f. = 1075; $F = 256$; $P < 0.001$). A typical section shows highest

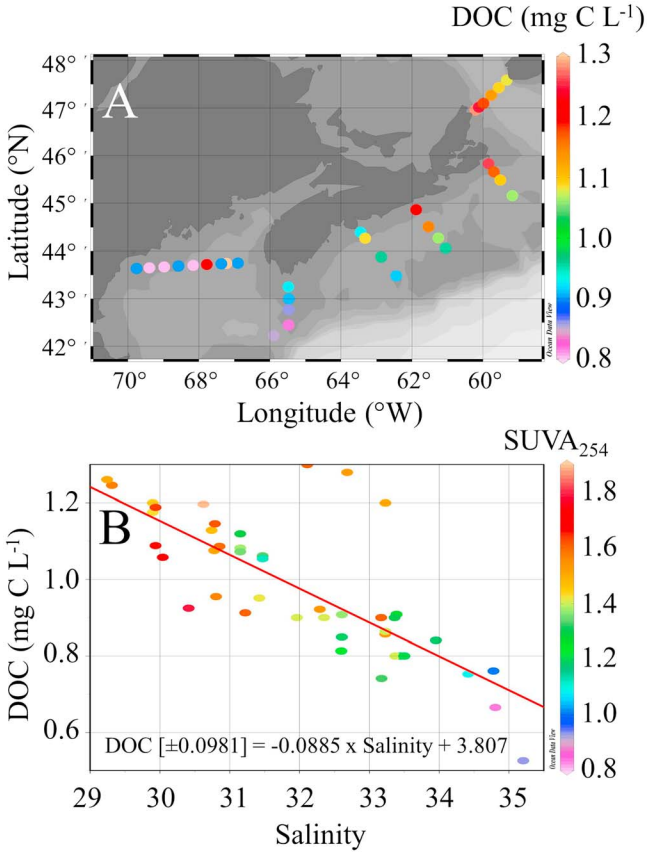

Figure 5. DOC concentrations measured during simultaneous GNATS and AZMP cruises during fall 2012 in Gulf of Maine, east coast of Nova Scotia, and waters north to Cabot Strait. (a) Map showing distribution of surface data. Regional distribution shows highest DOC concentrations leaving the GoSL and trending southwestward, with concentrations decreasing into the Gulf of Maine. (b) DOC concentration plotted against salinity with the color of the data indicating the specific UV absorption ($SUVA_{254}$). Data show increasing DOC and $SUVA_{254}$ at decreasing salinities. RMS error of the least squares linear fit is ±0.1 mg C L^{-1}.

concentrations (350 μg L^{-1}) within 50 m above the seafloor with numerous fine-scale plumes. There was often a large plume of POC-rich water (200–300 μg L^{-1}) extending upward from the seafloor to the surface from 68.4 to 68.8°W longitude, near Skate Bank, in the same region where the ExtEMCC crosses the GNATS transect. This plume of POC-rich water (250–300 μg L^{-1}) was 20 km wide. There also is a more shallow subsurface POC maximum at 25–30 m in JB waters (200 μg L^{-1}), which "outcrops" at the surface in the ExtEMCC and at 67°W.

Glider sections were integrated uniformly from 66.75°W to 69.8°W to a depth of 100 m in order to compare GNATS water column DOC and POC over the different missions (each with eastbound and westbound sections). Integrated DOC and POC (both in g C m^{-2}) are shown (Figures 7c and 7d). Overall, the results show that integrated DOC surpassed integrated POC by about 6 times. Moreover, there was strong temporal stability in integrated DOC and POC. Integrated DOC (Figure 7c) varied only ~9% over the 6 years that gliders were deployed across the gulf, while POC varied about 15% (Figure 7d).

In order to look at spatial trends of all the glider sections, the data were bin averaged to 0.1° longitude (along track) and 10 m depth bins in the vertical (Figure S3). Hydrographic results showed that on average, salinities were lowest (32) in the west shallow WMCC waters with a freshwater lens extending eastward. Greatest salinities (>34) were observed in deepest (180–200 m) waters in the Eastern GoM. Skate Bank separated the deep, high-salinity water of the east gulf from the deep, western portions (Figure S3A). Average temperatures were coolest in the deep waters of the western gulf, with warmest temperatures associated with the shallow, low-salinity lens that extends across the gulf. The deep, high-salinity water on the eastern side of the gulf was associated with 9°C water (Figure S3B). Densities of deep GoM water approached 27.5 (sigma theta). The 26.25 density surface sloped downward to the west across the entire transect, and, as with the salinity and temperature distributions, Skate Bank separated the highest-density deep water in the east from the western, deep portions of the GoM (Figure S3C). Moreover, water over Skate Bank showed the presence of 26.2 sigma theta water extending from 95 to 150 m depth. Water column stability (Brunt-Väisälä frequency; Figure S3D) was greatest in the surface, western gulf at depths <20 m (>1.4 cph). The aforementioned region of isopycnal mixing over Skate Bank was associated with low stability (0.9 cph). Waters 20–50 m above the sediments showed even lower stability (as low as 0.6 cph). Waters within JB showed moderate stability (1.2 cph) from 160 m to the surface, and waters on the eastern side of the transect showed Brunt-Väisälä frequencies of 1 cph (Figure S3D).

Bio-optical variability was strong over the GNATS transect. DOC sections showed the same monotonic tongue of water extending from the shallow western portions of the gulf eastward (Figures 7a and S3E). However, the

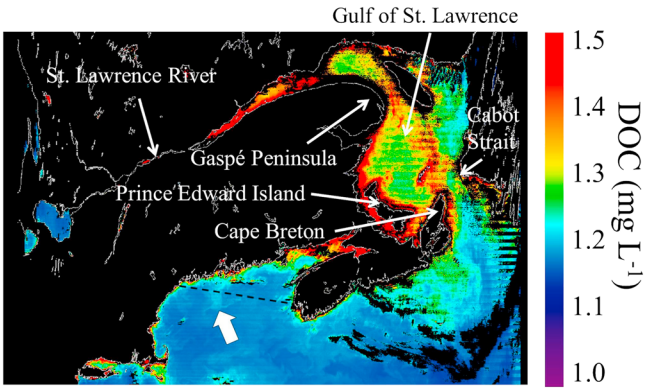

Figure 6. Image of regional DOC in the GoSL and GoM based on the adg_412_gsm product of MODIS Aqua (granule A2005275172500.L1A_LAC; 2 October 2005). Image was taken following a massive precipitation event which impacted NE North America. DOC concentration was based on the a_{g412}-to-DOC conversion given (Figure S1A) (based on GNATS data). Statistics for the relationship are $y[\pm 0.908] = 0.412[\pm 0.112]X^2 + 0.4733[\pm 0.272]X + 1.140[\pm 0.102]$; $r^2 = 0.331$; d.f. = 310; $F = 76.7$; $P < 0.001$ (Figure S1A). White arrow indicates the extension of the Eastern Maine Coastal Current which crosses the GNATS transect as it flows offshore.

average binned data also showed elevated DOC in the benthic layer in the western gulf, some 20 m above the seafloor. Average POC concentrations (Figure S3F) showed lowest concentrations at middepth of the JB, and highest concentrations 20–40 m above the seafloor, clearly biased to the western gulf. Waters of the ExtEMCC over Skate Bank showed evidence of elevated particle concentrations up to 100 m off the bottom. DOC:POC ratios approached 7 in the quiescent intermediate waters over JB, with values as low as 3 overlying the sediments, especially on the western portion (Figure S3G). Average chlorophyll fluorescence distributions showed highest values associated with the subsurface chlorophyll maximum at 20 m, in the WMCC and JB waters, with high values mixed to the surface in the SS waters and ExtEMCC waters. There was subtle low-level fluorescence variability at depth, with lowest values in the JB below 140 m (Figure S3H).

4.6. Spatial and Temporal Variability in Surface Chromaticity

The average annual chromaticities calculated from GNATS radiances showed that average colors of the water were consistent with FU values of 4–18 (pure colors of 485–575 nm), distinctly greater than those observed by Bigelow in 1912–1913 with FU values of 4–9 (pure colors 485–555 nm; Figure 8a). Changes in the average spectral radiance along the GNATS transect were also estimated using the SAS-derived nLw(λ) values during GNATS. The mean maximum nLw was about 510–520 nm in the region west of 68.8°W longitude (the WMCC and ExtEMCC), while waters of the JB averaged ~492 nm until the eastmost location directly adjoining Yarmouth, NS (Figure 8b). Note that the error bars in this plot are standard errors, which are small due to the large sample size (also given in the figure). Thus, for much of the data, with 600–800 data points, the standard deviations will be 25–30 times larger.

The location of the GNATS data in colorimetric coordinates show that for most of the data set, the annual, above-water, average gulf-wide spectral locus spanned from blue to yellow-green for GNATS results (FU levels 4–18), while the results from Bigelow data along the same transect (1912–1913) spanned from FU levels 4–9 (Figure 8a). This figure also shows the FU water types for *Wernand and van der Woerd* [2010], but as with Figure S3B, the error bars are standard errors resulting from 1000 to 3000 data points; hence, the standard deviations will extend across a far broader spectral range. Three years of the GNATS color data (2007–2009) show colors at or near the pure white point in the chromaticity plot (where all three of the tristimulus functions equal 1/3). These correspond to the 3 years that measurements were made on the high-speed *CAT* ferry (see section 5).

The normalized water-leaving radiance (nLw) spectra were examined gulf-wide between June and September (months sampled in all years of GNATS) for each year of the time series. The average peak wavelength of the nLw was higher on the western and eastern ends of the GNATS transects (greener colors) (Figure 8b). Examining the above-water spectral data by time showed increasing average peak wavelengths of the nLw from 493 to 514 nm (blue to green) between 2000 and 2006 and reduced peak wavelengths (green to blue) from 2013 to 2014 (Figure 8c).

4.7. Temporal Variability in Inherent Optical Properties

Inherent optical properties (IOPs) were also averaged through time during GNATS. Values of a_{g412} generally increased from the year 2000 (when dissolved ac-9 measurements were begun) until 2009. CDOM

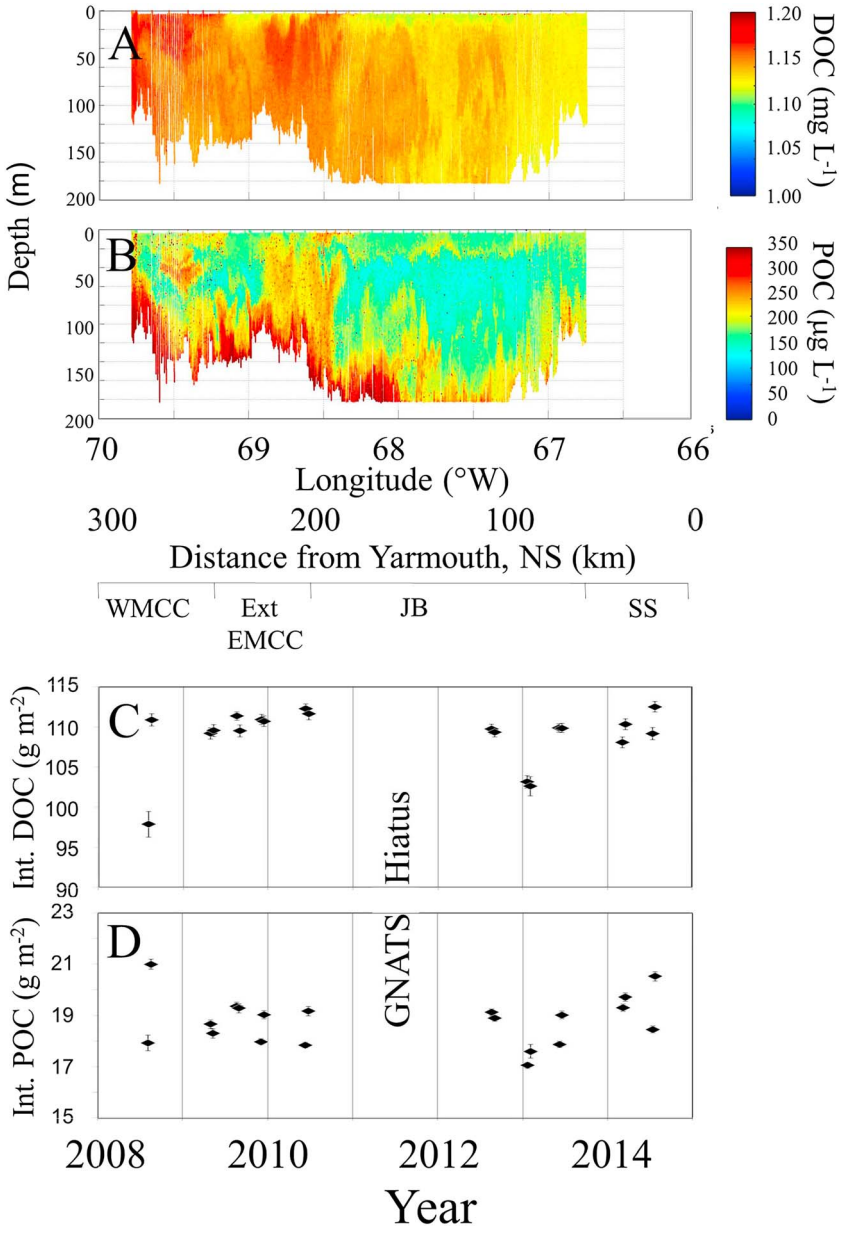

Figure 7. Glider data for GNATS. (a) Example of DOC data (units in mg C L^{-1}; based on CDOM optical proxy) for Mission 11, westbound leg. (b) Example of POC data (units µg C L^{-1}; based on particle backscattering optical proxy) for Mission 11, westbound. (c) Integrated DOC from 0 to 100 m, gulf-wide for glider missions (units in g m^{-2}; based on CDOM fluorescence to DOC optical proxy determined with parallel CDOM fluorescence and DOC samples). Note that missions 2, 3west, and 8 were incomplete and are therefore not shown. (d) Integrated POC from 0 to 100 m, gulf-wide (units in g C m^{-2}; based on b_{bp} to POC optical proxy determined for entire GNATS ship data set). For both Figures 7c and 7d, *Y* error bars are standard errors about the mean for all glider profiles, eastbound or westbound, respectively.

absorption dropped sharply in 2010 and then rose again in 2012, decreasing up until 2014 (Figure S4A). The sum of CDOM and detrital dissolved absorption (a_{pg412}) showed a similar increasing trend from 1998 to 2009, a precipitous decline in 2010 followed by increases again from 2012 to 2014 (Figure S4B). The time series of annual average gulf-wide scattering (defined as attenuation − absorption, $c - a$) of <0.2 µm micron material (b_{g412}) was close to zero from 2000 to 2003 before sporadically increasing and decreasing over subsequent years (Figure S5A). CDOM plus detrital scattering at 412 nm (b_{gp412}) was stable at ~0.6 m^{-1} until 2005 after which it rose to its highest value in 2009, decreased to lowest value in 2010, and increased thereafter (Figure S5B).

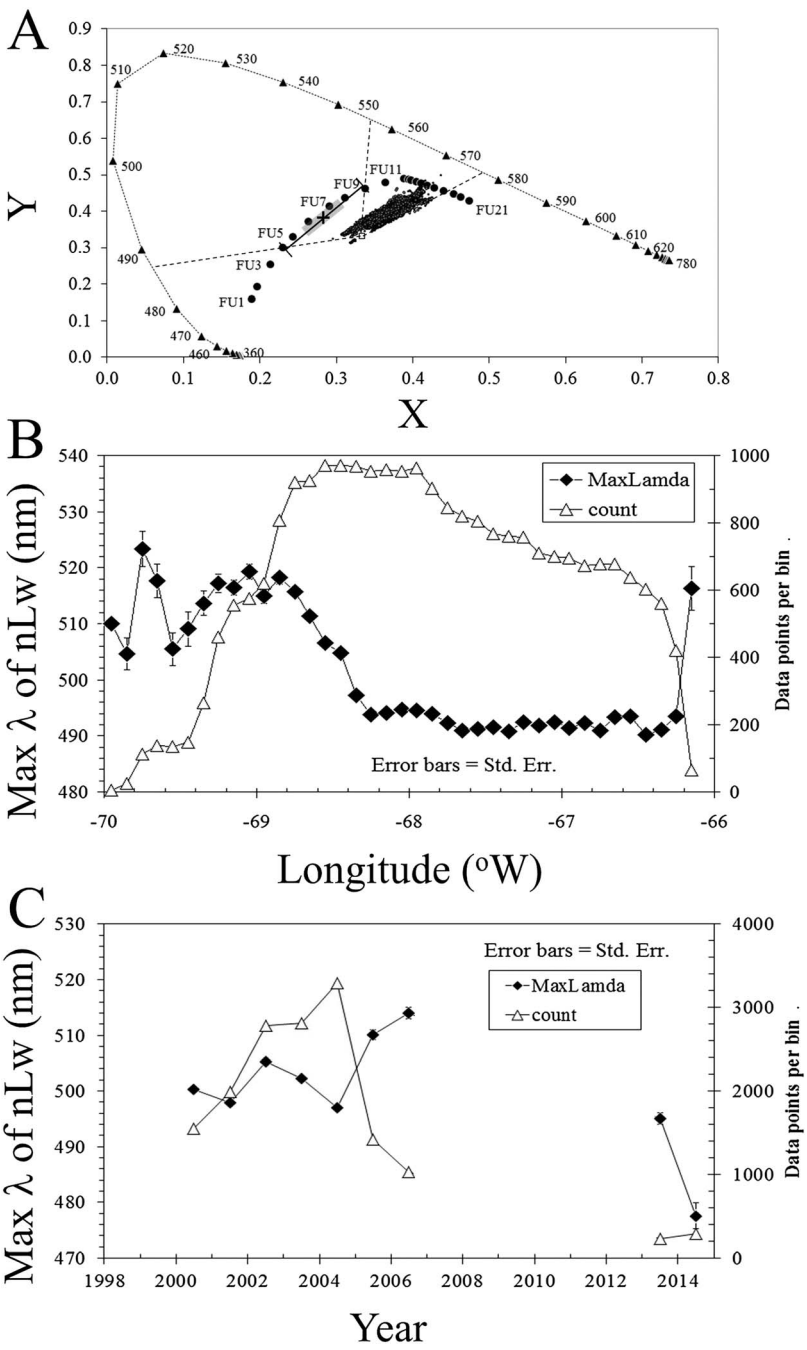

Figure 8. Chromaticity calculations based on GNATS above-water radiance data. (a) Chromaticity plot showing GNATS data (small cloud of black dots; $n = 21,572$), and Forel-Ule (FU) color scale (large solid dots; taken from *Wernand and van der Woerd* [2010]). *X* and *Y* refer to two of the three (tristimulus) functions for color perception in the human eye, where knowledge of any two allows calculation of the third [*Mobley*, 1994]. FU measurements from Bigelow from 1912 to 1913 ($n = 58$; *Bigelow* [1924]; range = 4–9; average = 6.59 ± 0.92) are shown with a "whisker plot." See text for details of chromaticity calculations. The saturated "white point" (where *X* and *Y* are 1/3) is shown for reference (open square). Pure colors are given around perimeter (black triangles). The two leftmost dashed lines illustrate the range in pure color for the Bigelow 1912–1913 observations (485–555 nm). The leftmost and rightmost dashed lines illustrate the range of pure colors representative of the GNATS observations (485–575 nm). (b) Maximum wavelength of the reflectance spectra binned according to longitude across GNATS transect. Numbers of observations are shown with open triangles. Error bars represent standard errors about the mean. Data for this plot include all seasons. (c) Maximum wavelength of the reflectance spectra binned to year. Since the period of June to September is common to all years sampled during GNATS, the means shown here are for only that period. Numbers of data per bin are shown with open triangles. Results from the GNATS cruises aboard the CAT ferry are not included due to the reasons discussed in the text.

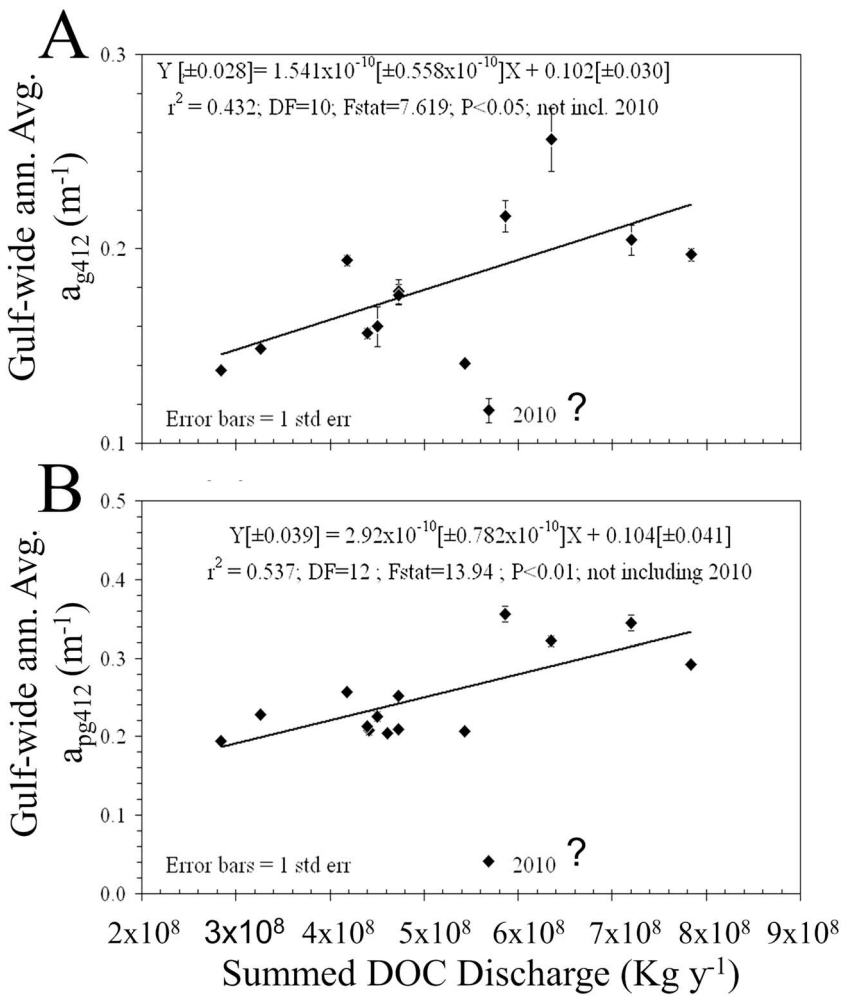

Figure 9. Plot of gulf-wide absorption between June and September plotted against river DOC discharge by 10 largest rivers emptying into the Gulf of Maine (calculated from LOADEST; see text). Absorption shown for (a) CDOM (a_{g412}; m^{-1}) and (b) CDOM plus detrital absorption (a_{gp412}; m^{-1}). Anomalously low datum from 2010 is not included in the regressions (see also Figures S4 and S5). Standard error bars shown about each datum unless they are smaller than the symbol. Linear, least squares fit and associated statistics are given in the figure, with standard error terms for each fit coefficient shown in square brackets.

4.8. Relationship of CDOM and Detrital Absorption to River Discharge

The average gulf-wide CDOM absorption (a_{g412}) from the GNATS was significantly related to river discharge from the 10 largest gauged rivers at ($P < 0.05$; Figure 9a) with medium correlation ($r^2 = 0.43$; least squares linear fit equation shown in panel). However, it should be noted that the anomalous datum for 2010 is not included in that regression due to lack of adequate ferry sampling that specific year. Regressing both dissolved and detrital absorption (a_{gp412}) against the combined river discharge from the 10 largest gauged rivers improved the fit (but again not including the anomalously low 2010 value in the regression) (Figure 9b).

4.9. Lagged Correlations Between River Delivery of DOC and GoM Optical Properties

CDOM absorption (a_{g412}) was also derived from MODIS Aqua data using the GIOP algorithm at four of the NERACOOS buoys, E, F, I, and M (Figure 1). These were compared to the DOC discharge from the five largest rivers from the Penobscot to the St. John Rivers discharging to the GoM (Penobscot, Narraguagus, Dennys, St. Croix, and St. John Rivers, rivers most impacting the NERACOOS buoy sites due general circulation (Figure 1)). The data were examined by comparing either weekly or monthly averaged data for both satellite-derived a_{g412} and river DOC discharge. The correlation, r, was calculated between weekly satellite-derived a_{g412} averages and weekly DOC river

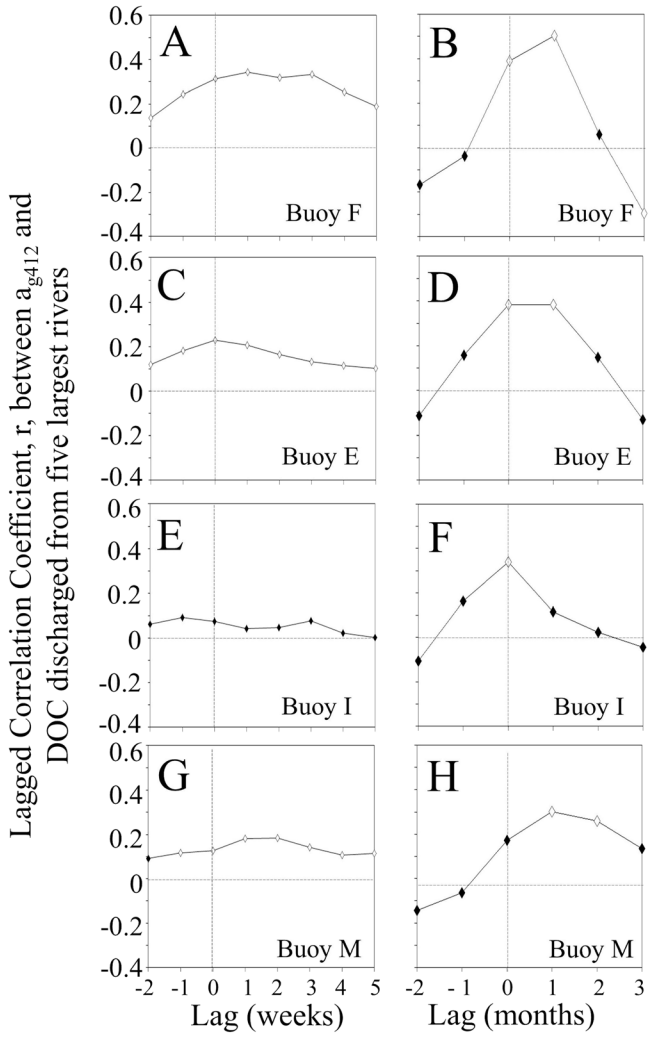

Figure 10. Lagged correlation coefficients (*r*) for MODIS Aqua-derived a_{g412} at four NERACOOS buoy locations (buoys E, F, I, and M; positions as shown in Figure 1) and DOC discharge estimates (from the five largest rivers, Penobscot, Narraguagus, Dennys, St. Croix, and St. John Rivers; see text for description). Correlations (a, c, e, g) for weekly binned data and (b, d, f, h) for monthly binned data where both MODIS and river discharge data sets were binned at the same time period. Open symbols represent significant correlations (for alpha, two-tailed distribution of $P < 0.05$) based on the *F* distribution for each correlation. Filled symbols represent non–statistically significant correlations.

discharge data (Figures 10a, 10c, 10e, and 10g). Correlations were also examined for monthly averaged satellite-derived a_{g412} and monthly DOC discharge data (Figures 10b, 10d, 10f, and 10h). Lag correlations were calculated from −2 to +5 weeks or −2 to +3 months, respectively. Negative lags were included in order to account for the possibility of spurious correlations. The highest correlation between river DOC export and satellite-derived CDOM was determined at the mouth of Penobscot Bay (NERACOOS buoy F). Indeed, maximum correlations were observed between 2 and 3 weeks using the weekly data or 1 month using the monthly data (Figures 10a and 10b). Correlations between CDOM and river discharge at buoy E (located near Monhegan Island, ~26 km from buoy F) were lower, and greatest correlations were observed at 0 weeks or 0–1 month, respectively (Figures 10c and 10d). At NERACOOS buoy I (east of Penobscot Bay, in the EMCC), there were no significant correlations using the weekly averages and only a zero month lag for the monthly data. For the NERACOOS buoy M in JB waters, significant but low correlation was observed at 1–3 weeks and 1–2 months, respectively.

When the average DOC across the GoM was estimated in the top optical depth using satellite imagery and regressed against summed DOC discharge from the five largest rivers discharging into the GoM (Penobscot, Narraguagus, Dennys, St. Croix, and St. John Rivers), overall correlations were low but significant. Greatest correlations ($r^2 = 0.29$) were observed using a 6 month lag (Figure S6; least square linear fit equation and statistical significance given in Figure S6A; $P < 0.001$). When the entire time series of DOC discharge by rivers was plotted next to the average DOC for the GoM, derived from MODIS Aqua, there was general alignment of the peaks (Figure S7). Upon applying a 6 month moving average to both data sets, there was improved correspondence in the peaks and troughs.

4.10. Future Projections of DOC Export

The LOADEST model was applied to the Penobscot River as described in section 3. The model calculations assumed stationarity in the factors that affect the export of DOC from rivers (such as the concentration discharge relationship through time). The predicted DOC export (kg C yr^{-1}) had the following least squares fit when plotted against year: DOC export $[\pm 2.67 \times 10^7] = 4.27 \times 10^5 [\pm 1.293 \times 10^5]$ Year $- 7.506 \times 10^8 [\pm 2.663 \times 10^8]$

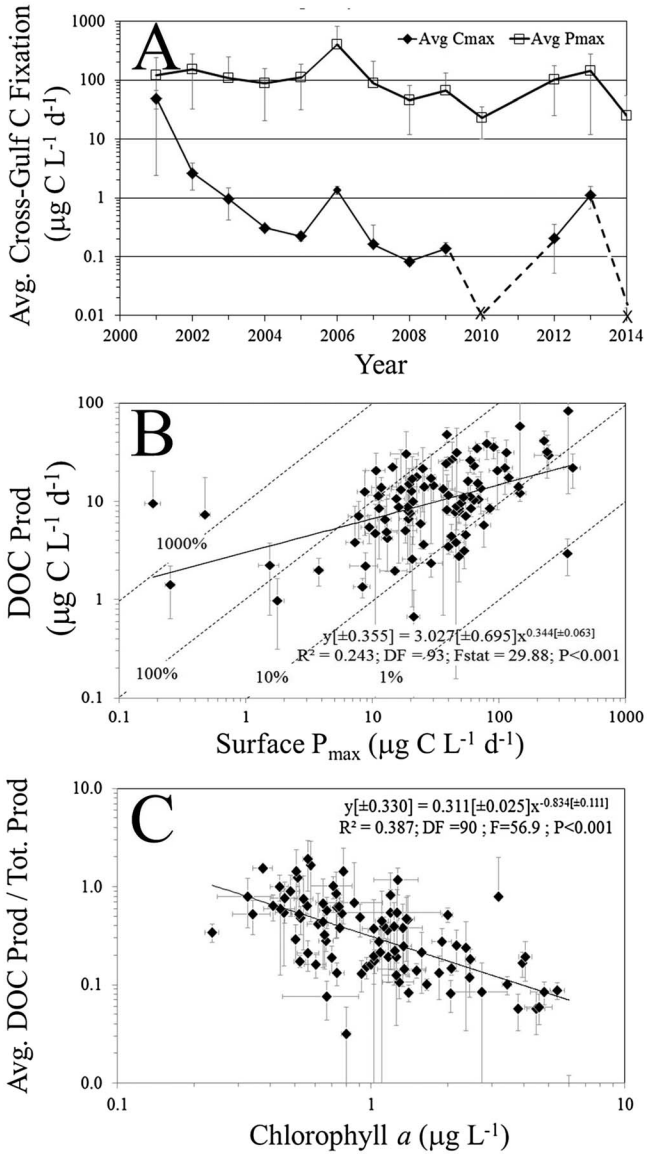

Figure 11. Carbon fixation rates into particulate and dissolved material in the GoM samples along GNATS transect. (a) Average cross-gulf, surface photosynthesis (open squares) and calcification (solid diamonds) from GNATS time series. Data only shown for the period of June–October (commonly sampled period for all years). Seawater samples incubated at surface light intensities for 12 h (see supporting information for methods). Error bars represent standard deviations. Calcification during 2010 and 2014 were below 0.01 mg C L^{-1} d^{-1} (near the limit of detection of the method) so data are shown with crosses along the abscissa. No data were available for 2011 due to a hiatus in the GNATS program. (b) Results of ^{14}C-DOC measurements from GNATS made between 2012 and 2014 (all months) showing surface DOC production rate plotted against P_{max} rates (both in µg C L^{-1} d^{-1}). Error bars represent standard deviations of triplicate measurements. Dotted lines represent the ratio of DOC production: primary production (in %). Least squares fit to the data also shown with solid line. Statistics of regression are shown in lower right of panel. Standard errors of fit parameters are given in square brackets. (c) Average DOC production/total production in GNATS samples between 2012 and 2014, plotted against chlorophyll *a* concentration. Error bars represent standard deviations of triplicate measurements. Least squares fit equation shown in upper right of panel with standard errors of parameters shown in square brackets.

(where values in square brackets represent the SE of the fit terms). The statistics for this linear regression show a statistically significant relationship (d.f. = 78; $r^2 = 0.12$, $P < 0.005$). With the given variance, the relation predicts a substantial increase in DOC export over the next 80 years (Figure S8).

4.11. Other Sources of DOC to the Gulf of Maine

Dissolved organic matter is also released from phytoplankton during normal growth. Primary production and calcification have both shown strong decreases over the GNATS program (Figure 11a); note the log scales and that calcification fell below the abscissa during 2010 and 2014 (signified by the crosses in Figure 11a). During 2012–2014, overall DOC production decreased as a function of the measured surface maximum photosynthesis (P_{max}; regression shown in the Figure 11b; $r^2 = 0.243$; $P < 0.001$; Figure 19b). Isopleths of the DOC release as a fraction of the total surface P_{max} are also shown in Figure 11b. The least squares regression line trended to an increasing fraction of DOC release as the productivity dropped. Most of the data, however, fell between 10 and 100% of production released as DOC. The data were rearranged to show the ratio of DOC production/P_{max} as an inverse power function of chlorophyll$^{-0.83}$ ($r^2 = 0.39$; $P < 0.001$; Figure 11c).

5. Discussion

5.1. Gulf of Maine River DOC Discharge Trends

The variance in interannual DOC discharge as estimated from LOADEST for the 10 largest GoM water sheds was too large to be able to discern whether there has been a significant increase in discharge since the intensive GNATS sampling began in 1998 (Figure 2a). However, the record-setting rainfall in 2005 plus the increase in CDOM observed in

coastal Maine waters in 2005 (relative to the early years) suggested higher than normal DOC modeled discharge in the latter part of the sampling program [*Balch et al*., 2012]. Another reason that a significant linear trend is not evident in the LOADEST-derived DOC discharge into the GoM over time (Figure 2a) is that rainfall levels in 2012 and 2013 were lower than those observed in 2005, 2006, 2008, 2009, and 2011 (most years between 2006 and 2011); hence, there was not as much runoff for moving the DOC from land to sea. Nonetheless, the variance in precipitation has increased over time during the period of the GNATS [*Balch et al*., 2012], which likely led to the high variability in the DOC discharge (consistent with trends observed by *Tian et al*. [2015]). Unlike the 15 year time series above, DOC export predicted by LOADEST over 84 years in the Penobscot did show a significant 30% increase in DOC export rate (Figure 2b). Moreover, the decadal statistics showed a linear increase in both the mean and variance of the estimated Penobscot DOC discharge. While decadal mean DOC discharge estimated by LOADEST increased ~30%, the decadal variance in Penobscot River DOC discharge increased 230% (Figure 2c). *Tian et al*. [2015] showed (using a modeling approach) that the standard deviation in DOC flux estimated between 1979 and 2008 for watersheds of the eastern U.S. were 167% greater than the standard deviation observed between 1901 and 1930. This is also consistent with other previous estimates of changes in the climatology of the region. Using a 100+ year precipitation data record from three weather stations in Maine flanking the Penobscot Estuary, the variance in measured precipitation was shown to have almost doubled [*Balch et al*., 2012]. Combining these results with the current observations, it appears that factors that affect the quantity of river discharge do indeed affect the DOC export rates into the near-shore waters [*Huntington and Aiken*, 2013]. That is, DOC export is limited more by water availability than DOC production (mineralization of DOM and leaching). It is difficult in the GoM watershed to attribute such long-term variability to change in land use/land cover (which have been minimal in the last century in the GoM watershed), whereas the data show that precipitation and temperature have increased significantly [*Balch et al*., 2012; *Tian et al*., 2015].

5.2. Optical Prediction of DOC From Space-Based Measurements

Prediction of DOC concentration based on blue (412 nm) absorption is not possible in the open ocean since CDOM is uncorrelated to DOC due to photooxidation and remineralization [*Siegel et al*., 2005] and open ocean DOC lacks the optically active aromatic compounds characteristic of terrestrial runoff. However, in coastal waters this is not the case so that satellite remote sensing can help define DOC budgets from space [*Del Castillo et al*., 2001; *Mannino et al*., 2008], especially near rivers where there is typically a strong correlation between DOC concentration and CDOM absorption [*Ferrari et al*., 1996]. Our observations demonstrate that adding information from progressively shorter wavelengths in the UV, as well as spectral slope, improves the accuracy of GoM DOC predictions by a factor of 2 to an accuracy of ±0.42 mg C L^{-1} (Figure S1), in agreement with other recent studies [*Fichot and Benner*, 2011; *Fichot and Benner*, 2012; *Fichot et al*., 2008; *Mannino et al*., 2014]. From a remote sensing perspective, this is encouraging for the future NASA PACE mission (Pre-Aerosol Clouds and ocean Ecosystem) for launch in 2020 [*Del Castillo et al*., 2013]. PACE will be a well-calibrated and characterized sensor with a spectral range of 350–800 nm with ~5 nm wide bands. Our results here demonstrate that the gain in accuracy in predicting DOC from 350 nm to 254 nm is incremental, since the DOC accuracies only improve by 7% (Figures S1B and S1C). The strongest advance for estimating DOC will be combining UV absorption measurements with measurements of spectral slopes (Figure S1d).

5.3. Covariance of Spatiotemporal Patterns of DOC and CDOM

The relatively good covariation between our measurements of a_{g412}, a_{gp412}, and DOC (Figures S1A, S2A, and S2B) allow for the accounting of low but significant variance of DOC concentration (33%) using optical proxies at 412 nm. The mean, gulf-wide trends in a_{g412} and a_{gp412} demonstrate that the particulate detrital component of this absorption may represent at most about 0.1 m^{-1} absorption (~15% of the total absorption in western GoM waters) and that the three peaks in both are associated with the water masses WMCC, ExtEMCC, and the SS (Figures 1 and 3). Upwelling associated with frontal boundaries between water masses remain a likely source of CDOM, too, which, due to the recent surfacing, has not been photobleached. This is probably most true at the ExtEMCC where earlier studies showed that the tip of the plume was associated with anticyclonic vorticity, leading to doming of temperature and salinity isopleths (as well as a source of new nitrogen to the surface) [*Pettigrew et al*., 1998]. The double peak in a_{g412} shown near 69°W (Figure 3) is likely due to the fact that the position of the ExtEMCC is not always crossing the GNATS transect at the same location.

The GoM was previously classified as a primarily Case II-dissolved water body all the time, and Case II-particulate about half the time [*Balch et al*., 2004; *Yentsch and Phinney*, 1997]. The dominance of CDOM absorption here would continue to buttress that conclusion. However, we have now documented a dissolved (<0.2 μm) scattering component, too, and the mean distributions show a strong enhancement not just in the coastal waters but occasionally across the GoM (Figure S2F). Earlier in our GNATS work, we showed the increasing b_{g412} in coastal waters [*Balch et al*., 2004] with values averaging 0 to 0.3 m^{-1}, reaching values of 0.6 m^{-1} in the western gulf (Figure 4a). This is entirely consistent with the trends observed through many more years of sampling as shown here, with lowest values in the middle of the GoM (~0.2 to 0.3 m^{-1}) and average values increasing to 1.1 m^{-1} in the western gulf coastal waters (Figure 4a). The b_{g412} pattern also covaried with a_{g412} (Figure 4a inset) suggesting that this material was somehow associated with CDOM and/or terrestrially derived DOC. Such particles <0.2 μm might also be expected to show elevated backscattering, too, since particles <1 μm are responsible for the majority of the backscattering [*Morel and Ahn*, 1991; *Stramski and Kiefer*, 1991].

Unfortunately, dissolved backscattering was not measured in GNATS. Previous measurements of backscattering for <0.2 μm water in the equatorial Pacific Ocean showed low but measurable values [*Dall'Olmo et al*., 2009]. More recently, *Zhang and Gray* [2015] have demonstrated strong backscattering by <0.2 μm diameter particles in coastal regions of the Gulf of Mexico and mid-Atlantic Bight which accounted for 40–80% of the total backscattering at 532 nm but at most 5% of the total particle scattering. Our estimates of b_{g412} represented a larger fraction of the total scattering at 412 nm (>40% of b_{pg412}; Figure 4), with spatial distributions across the entire 300 km GNATS transect. We can only surmise that the composition of these <0.2 mm particles is different in the GoM than in the Gulf of Mexico or Mid-Atlantic Bight as observed by *Zhang and Gray* [2015]. However, it is also notable that in *Zhang and Gray* [2015], b_{g412} was also correlated to CDOM absorption (a_{g412}), similar to our observations.

Typically, the scattering of CDOM is assumed to be zero in the sea [*Mobley*, 1994; *Vaillancourt et al*., 2005]. The nature of this material measured in GNATS is not known, although given its size (<0.2 μm), it might have been associated with microgels which self-aggregate from nanometer-sized particles into submicron and micron-sized particles [*Orellana et al*., 2007]. Flocculation of particles can also occur associated with the mixing of low-salinity river water with higher-salinity marine waters [*Chen et al*., 2005; *Wolanski and Gibbs*, 1995]. This might explain the largest peak of b_{pg412} associated with the western extreme of the transect, in the WMCC (Figure 4b), also with highest CDOM (Figure 3; representing a source of DOC). The peak in b_{pg412} in the ExtEMCC (Figures 1 and 4b), greater than b_{g412}, may represent the upwelling of neutrally buoyant nepheloid particles that can be found deeper in the water column [*Gardner and Sullivan*, 1981; *Pak et al*., 1980; *Spinrad et al*., 1983]. There is clear evidence of this upwelling in the glider sections of POC (based on b_{bp}; Figure 7b) where the normally 30–50 m thick nepheloid layers appear to be mixed to the surface at the position of the Skate Bank and the ExtEMCC with its associated upwelling.

5.4. Interpretation of Results From the Laurentian Channel and East Scotian Shelf

Ship-based DOC measurements from the NE Atlantic, off Nova Scotia, show a tongue of elevated DOC water emanating from the Gulf of St. Lawrence at the Cabot Strait and trending with the low-salinity GoSL water along the coast of Nova Scotia. To the extent that we saw low-salinity, elevated CDOM water at the eastern end of the GNATS transect (Figures 3 and S2C), this evidence points to a GoSL source, especially when combined with ship measurements (Figure 5a) and remote sensing imagery (Figure 6). Generally, the surface DOC concentration in the region follows a quasi-conservative mixing line from salinities of 35.5 to 29 (a drop of 18%) (Figure 5b), suggesting one primary source. However, over this salinity range, $SUVA_{254}$ dropped 55% from 1.8 to 0.8 suggesting that the initial CDOM was of terrestrial origin but that the composition changed nonconservatively. This would be expected since CDOM in surface waters could have been photooxidized enroute to the Gulf of Maine as well as vertically mixed [*Opsahl and Benner*, 1998]. Earlier work of *Smith et al*. [2001] suggested that it took about a year for GoSL water to travel to the GoM; hence, photooxidation remains a distinct fate for surface CDOM. The satellite view of the CDOM distribution (Figure 6) agreed with this interpretation with the influx of low CDOM/DOC oceanic water along the northwest portions of GoSL and discharge through Cabot Strait, along the coast of Cape Breton. The GoM showed general enhancement of DOC along the northwest portions, presumably due to increased river input. Indeed, the satellite view of DOC in the ExtEMCC agreed with the previously described position of

the current derived from Advanced Very High Resolution Radiometer, showing filaments extending into both WB and JB [*Pettigrew et al*., 1998] (see arrow in Figure 6).

5.5. Vertical Section Data Along the GNATS Transect

The glider data provided insight into the sources of CDOM and particles into the gulf. Temperature and salinity sections show the origins of warm, salty North Atlantic slope water entering through the Northeast Channel [*Ramp et al*., 1985]. The resulting density distribution shows the 26.25 sigma theta isopycnal sloping downward toward the west, indicating the southward baroclinic flow of the ExtEMCC and WMCC (Figure 7c). The average density distribution actually shows evidence of strong mixing over Skate Bank (at about 68.8°–69.2° W longitude along the GNATS transect), with low stratification (Figures S3C and S3D). A tongue of DOC confined to the western GoM showed that mean concentrations were highest in the westmost surface waters and strongly suggests the predominant riverine source of the optically active CDOM. Moreover, the relatively low values of DOC in surface waters (Figure S3E) may have been an artifact of basing the DOC estimate on CDOM fluorescence with changing excitation/emission properties or changes due to photobleaching in surface waters. The stability in both DOC and POC integrals (Figures 7c and 7d) was probably due to the fact that the DOC contributed by rivers was still a relatively small fraction of the total DOC in the GoM system, where inflowing DOC concentrations through the Northeast Channel were 1.1 mg C L^{-1}, while the rivers are supplying DOC as a point source at the surface near the coast. Moreover, the deeper nepheloid POC (assumed to be mostly nonliving) dominated variability of the integrated total suspended POC to 100 m (Figure 7b).

The vertical POC estimates defined by the gliders (based on the b_{bp532} proxy measurements) shows little relation to the DOC distribution, suggesting that river-borne particulate matter is probably not a dominant source of particulate matter to the GoM. This may appear contradictory to our previous observation that gulf-wide average POC is directly related to river discharge; that is, as river discharge increases, so does the gulf-wide average POC concentration. However, that correlation accounted for only 50% of the variance [see *Balch et al*., 2012, Table 1]. Other factors are contributing POC to the gulf (e.g., aggregation and flocculation). Particle backscattering (hence POC) shows the strongest source function over the sediments, with striking upward mixing and seeding of benthic particles into surface and chlorophyll maximum waters (e.g., Figure 7b; see also *Pilskaln et al*. [2014]). Despite the apparent injection of benthic particles upward in the water column, DOC remains the predominant organic carbon fraction across the GoM, even in nepheloid-rich bottom waters (Figure S3G). Interannual variability of the massive DOC pool is only about 5%, due to the small river discharge relative to the large integrated DOC pool in the GoM (Table 3).

5.6. The Timing of DOC Injections Into the Gulf of Maine

The time lag between the LOADEST DOC discharge estimates and the appearance of the DOC (based on the CDOM proxy measurements of a_{g412} from MODIS Aqua) at the various NERACOOS buoy sites was always higher for data binned on the monthly time scale than weekly binned data. This is probably due to variance associated with other high-frequency processes that might affect the displacement of the CDOM (and DOC) as it moves away from the coast (e.g., fortnightly tidal cycles and wind mixing) which are averaged out at the monthly time scales. Moreover, the time lags for maximum correlation (between LOADEST-predicted DOC discharge and MODIS-derived satellite DOC estimates) were shorter for the coastal buoy sites (0–1 month) than the offshore buoy M site (1–2 months), which would be expected given the longer distance from the river mouths to the central gulf as well as the directions of advection of river water past the various buoys. Indeed, the 6 month binning time scale for peak correlation of LOADEST-predicted DOC river export with average surface GoM DOC (determined by satellite) would be expected since there are two major flushes of river DOC into the gulf each year, the spring freshet dominated by snowmelt and a smaller fall freshet, separated by approximately ~6 months [*Hodgkins and Dudley*, 2005]. The 6 month time period is shorter than the 1 year time scale for the turnover time of the gulf's waters [*Ramp et al*., 1985] presumably due to loss of CDOM from surface waters (via photooxidation or physical subduction and deep mixing). After buoyant CDOM-rich river water gets mixed seaward in the spring, the next time period to mix it deep into the water column would be the following fall during the breakdown of the seasonal pycnocline. Climate and hydrologic projections for this region [*Hayhoe et al*., 2007; *Thibeault and Seth*, 2014] suggest a strong likelihood of increasing precipitation and runoff that is consistent with the increases in precipitation and runoff observed since the early twentieth century [*Huntington and Billmire*, 2014]. This is also consistent

Table 3. Fluxes and Standing Stocks of DOC and POC in the Gulf of Maine and Resulting Constraints on Its Turnover[a]

Carbon Discharge/Production	(kg C yr^{-1})	Assumptions
River DOC discharge (10 largest rivers)	4.50×10^8	Stationarity of LOADEST model
River DOC discharge scaled to all watersheds	7.67×10^8	DOC discharge scaled to GoM watershed by multiplying by the ratio of the area represented by the 10 rivers at their gauging locations (179,008/104,475) or 1.713 (see Table S1)
Integrated net phytoplankton production of POC over GoM	3.97×10^{10}	Average annual net PP = 40 mg m^{-3} d^{-1}; 30 m euphotic zone; area of GoM = 90,700 km^2
Phytoplankton DOC production	1.19×10^{10}	30% loss of PP as DOC
Standing stocks	(kg C)	
Gulf of Maine DOC	1.50×10^{10}	Glider average DOC = 110 g m^{-2} over average depth of GoM = 150 m; area of GoM = 90,700 km^2
Gulf of Maine POC	2.58×10^9	Glider average POC = 19 g m^{-2} over average depth of GoM = 150 m; area of GoM = 90,700 km^2
Constraints	Miscellaneous Units	
Percent total DOC supplied by GoM watershed	6.1%	Based on above LOADEST estimates of river DOC discharge and measurements of DOC production extrapolated over GoM
Physical turnover time of GoM water	11 ± 2 months	*Ramp et al.* [1985]
Steady state turnover time of water column DOC	1.18 years	Sources balance sinks
Steady state turnover time of water column POC	23.8 days	Sources balance sinks
Ratio of phytoplankton DOC production/River DOC discharge	15	Based on above LOADEST estimates of river DOC discharge and measurements of DOC production extrapolated over GoM

[a]River DOC discharge, given as average of values for years 1998–2013 (Figure 2a), derived from LOADEST. Values assume stationarity of the values. Phytoplankton net POC production rate is the average based on GNATS measurements, applied over the top 30 m of the water column and over the area of the Gulf of Maine. Phytoplankton DOC production is based on measured ^{14}C-derived DOC production and primary production (Figure 11b) applied over GoM. Standing stocks of DOC and POC are based on glider-based estimates (using optical proxies; Figure 7). Constraint for the DOC supplied by the GoM watershed as well as the ratio of phytoplankton DOC production/River discharge is based on the total DOC exported from rivers and the measured phytoplankton DOC production extrapolated to the area of the Gulf of Maine, applied over the top 30 m depth. Turnover values of DOC and POC assume a steady state of each (such that sources balance sinks). PP, primary production.

with the roughly 30% increase in DOC that is being predicted by LOADEST and the HadCM3 general circulation model (GCM) over the next 80 years (Figure S8). However, the major assumption of stationarity in the factors affecting the LOADEST prediction must still be validated (T. Huntington et al., submitted manuscript, 2015).

5.7. A Century of Ocean Color in the Gulf of Maine

Wernand and van der Woerd [2010] have shown that the longest available record of ocean color comes from measurements against the FU color comparator scale observations (going back to 1890). Certainly, the Forel color data of *Bigelow* [1924] compared to the calculated chromaticity estimates made here (based on nLw), suggest a general "yellowing" of the GoM waters along the GNATS line over the last century. It should be noted that partial variability in chromaticity seen along the GNATS transect could be accounted for by longitude (water color further west was generally more yellow-green, in waters with reduced salinities (Figures 8b and S3A), reduced density (Figure S3C), and increased CDOM (Figure 3a)). The horizontal distribution of *Bigelow's* [1924] chromaticity data (not shown) and ours (Figure 8b) illustrate westward yellowing along the GNATS transect (see also *Yentsch and Phinney* [1997]). The temporal trends in the gulf-wide, maximum nLw wavelength observed over the duration of GNATS suggest high variance and a "yellowing" from 2000 to 2006. Data from 2007 to 2009 were not included in Figures 8b and 8c since they correspond to the years GNATS sampled from the high-speed *CAT* ferry, for which the chromaticity data were close to the white point on the chromaticity plot (not shown). The radiometers were aimed outside of the narrow bow wake of the *CAT* ferry, so they would not have viewed light scattering from bubbles in the ship's wake. Instead, there often were more marine aerosols and sea spray in the air around this fast-moving vessel that may have "whitened" the above-water reflectance measurements. Regardless, the a_{g412} and a_{pg412} data from these years showed *more* CDOM and detritus in the waters from 2007 to 2009 (Figure S4A).

Over the century time scale between Bigelow's work and our own, the observed yellowing based on the chromaticity plots, the positive correlation between GNATS averaged annual CDOM measurements, and river DOC discharge data (Figure 9), combined with LOADEST and GCM model predictions for higher DOC river

fluxes (Figure S8), all point to future yellowing of the GoM from CDOM, primarily associated with an increased intensity of the hydrological cycle, and more river discharge. While this prediction comes from only one GCM (instead of an ensemble average of multiple models), increasing precipitation and runoff over the northeast region has been forecast by others. *Hayhoe et al*. [2007] made a similar prediction based on several models. *Thibeault and Seth* [2014, Figure 6g] projected increasing precipitation over the region using 23 Coupled Model Intercomparison Project Phase 5 (CMIP5) coupled models, albeit this was done at coarse resolution and not small spatial scales. Nonetheless, there is consistency in projections of increasing precipitation with the CMIP5 39-model ensemble [*Collins et al*., 2013, Figure 12.22, p. 1078]. *Collins et al*. [2013] point out that the consensus on 21st century rainfall projections in climate models is more widespread than previously thought [*Power et al*., 2012]. In *Power et al*. [2012], the northeast U.S. is in a region where consensus is higher (except summer precipitation in June, July, and August). Indeed, the most uncertainty in rainfall projections is in the tropics and subtropics. Such an increase in CDOM runoff could have an impact on reduced GoM water transparency at the blue wavelengths, with ramifications to further potential decreases in phytoplankton photosynthesis and productivity [*Balch et al*., 2012].

5.8. Factoring in DOC Production by Phytoplankton

In the above analysis, we have focused on the export of DOC by rivers; however, DOC production by resident microflora cannot be ignored in this analysis. While our new results show a dramatic loss of productivity and calcification in the Gulf of Maine during GNATS after 2006 (Figure 11a), the results still demonstrate a typical loss of DOC from phytoplankton equivalent to 10–100% of the carbon fixed (Figure 11b) and that relative DOC production showed an inverse trend with chlorophyll concentration (Figure 11c). We would suggest that this is due to increases in the surface:volume ratio of the phytoplankton at progressively smaller cells. *Dussart* [1965] originally defined the operational size classes of the plankton. His three smallest size classes were divided into picoplankton (0.2–2.0 μm), nanoplankton (2.0–20 μm), and microplankton (20–150 μm). Based on our Flowcam observations (not presented here), nanoplankton dominate at the lowest chlorophyll levels. These extremes can be crudely approximated at the highest chlorophyll concentration; assuming 20 μm diameter, spherical, phytoplankton cells, the surface-to-volume ratio would be 0.30 μm^{-1}. For particles dominated by 2 μm diameter nanoplankton, the surface-to-volume ratio would be 3.0 μm^{-1}, 10 times larger. The DOC production/total production ratio that we observed in GNATS also increased about 1 order of magnitude, from high to low chlorophyll concentrations, close to the same magnitude we would expect based on an order of magnitude decrease in particle size and associated increase in surface-to-volume ratio (Figure 11c).

Assuming that an average of 30% of algal productivity is lost from phytoplankton, with an average euphotic zone primary production of 40 $\mu g C L^{-1} d^{-1}$ over the top 30 m, then the gulf-wide, annual, phytoplankton DOC production would be ~1.19×10^{10} kg C yr^{-1}, 15 times larger than the annual DOC discharge for the 10 largest rivers entering the GoM, scaled to the entire GoM watershed (Table S1). However, the CDOM/DOC distribution in the GoM reflects the most refractory, large molecular weight, colored, humic inputs from rivers (Figure S3) with an allochthonous source near the west side of the GNATS transect (and lesser GoSL influence on the eastern side in SS water). Algal-produced DOC is more labile, lower molecular weight, less aromatic [*Kirchman et al*., 1991], and less colored than terrestrially derived DOC. However, it is autochthonous, with a broader spatial distribution due to its broader source function. Thus, the CDOM-based DOC concentration clearly shows the westward bias in the GoM. If the CDOM-derived DOC concentration were considered steady state, and it was assumed that sources balanced sinks, the turnover of the DOC would be 1.2 years (Table 3), which slightly exceeds the physical turnover time of the GoM water of 11 ± 2 months [*Ramp et al*., 1985]. Thus, DOC is being flushed out of the GoM about as fast as it accumulates. POC turnover, on the other hand (based on the same steady state assumptions), would have a turnover time of 24 days; thus, this POC is being recycled within the GoM system before such material can be exported (this would include all sources of production ranging from algal production to flocculation as well as losses due to sinking).

5.9. Concluding Remarks

On average, DOC and POC export by global rivers are about 55% and 45%, respectively, of the total organic carbon fluxes [*Ludwig and Probst*, 1996]. *Wetzel* [1975] reported that a ratio of ~ 9:1 DOC:POC is transported in Maine and Maritime rivers, and this is supported by *Roesler et al*. [2006]. Our data suggest DOC:POC ratios of 7 in the eastern side of the GoM (of course, the high concentrations of DOC in seawater also will elevate this ratio). Increased salinities in the gulf will slow flocculation/sinking, too, thus keeping DOC concentrations

high. Our study shows that there is a submicron fraction of optically scattering material (flocculant material?) as well which appeared to be exported from the river continuum across the GoM during the extreme precipitation years from 2006 to 2010, along with the highly blue-absorbing CDOM (Figure S2). This was in agreement with *Bauer et al*. [2013], who described the disproportionate effect of individual events for moving terrestrial carbon to the sea, such as that observed by *Yoon and Raymond* [2012] where a single tropical storm exported 40% of the annual river DOC budget to the sea.

Wernand and van der Woerd [2010] suggested that FU color comparator measurements will provide us the longest record for understanding changes in the color of the ocean over century time scales. Indeed, there is a relatively large data base of such measurements which should be assessed to look at larger spatial-scale color changes than seen in the Gulf of Maine. We concur with this assessment as the best way to move forward with modern radiometric measurements in conjunction with the reintroduction of parallel FU measurements. Only then will we be able to statistically assess and compare changes in ocean color at the century time scale associated with land-to-sea carbon export.

Acknowledgments

We gratefully thank the captains, crews, and staff of the M/S *Scotia Prince*, *The CAT*, M/S *Nova Star*, R/V *Connecticut*, R/V *Argo Maine*, and F/V *Ella and Sadie*, who have facilitated the collection of the GNATS data set. Our work was also aided by numerous people who helped with the many GNATS cruises over the years (unless otherwise noted, these individuals are/were employees of Bigelow Laboratory): Danielle Alley, Emily Booth, Carl Boyd (Dalhousie University), Rosaline Campbell, Joaquim Goes, James Johnson, Emily Lyczkowski, Elise Olson, David Phinney, Carlton Rauschenberg, Nick Record, Bob Vaillancourt, Laura Windecker, Meredith White, and Charles Yentsch. Bill Li and staff of the Bedford Institute of Oceanography, Department of Fisheries and Oceans (Bedford, Nova Scotia) facilitated the sampling of DOC as part of an Atlantic Zone Monitoring Program cruise from Cabot Strait, the Laurentian Channel, along the east Scotian Shelf, plus Brown's Bank. The GNATS data used in this study are available from (NASA SEABASS; http://seabass.gsfc.nasa.gov/). Discharge and water chemistry data for gauging stations in the United States can be obtained from the National Water Information System (NWIS) online database (http://nwis.waterdata.usgs.gov/nwis/sw). Data from St. John at Mactaquac were obtained from New Brunswick Power (Michael Chiasson, dam operator). Discharge data for the St. John River at Mactaquac Dam are available from USGS digital files (Main Office of the New England Water Science Center, Augusta Maine, 04330). We gratefully acknowledge the support of NASA (biogeochemistry program) for maintaining the GNATS program since 1998 (NAS5-97268; NAS5-31363; NAG5-10622; NNG04GI11G; NNG04HZ25C; NNX07AD01G; NASA EPSCOREP-02-14; NNX08AB10G; NNX08AJ 88A; NNX10AT67G; NNX11AQ70G; NNX14AM77G). Additional support was generously provided by NOAA (40-AA-NE-005996). T.H. was supported by NASA grants NNYH04AA661 and NNH08A1571 and the U.S. Geological Survey funds for climate research. G.A. was supported by NASA grants NNX09AU89G and NNH04AA62I. Any use of trade, firm, or product names is for descriptive purposes only and does not imply endorsement by the U.S. Government.

References

Andrew, A. A., R. Del Vecchio, A. Subramaniam, and N. V. Blough (2013), Chromophoric dissolved organic matter (CDOM) in the equatorial Atlantic Ocean: Optical properties and their relation to CDOM structure and source, *Mar. Chem.*, *148*, 33–43.

Balch, W. M., D. T. Drapeau, B. C. Bowler, E. S. Booth, J. I. Goes, A. Ashe, and J. M. Frye (2004), A multi-year record of hydrographic and bio-optical properties in the Gulf of Maine: I. Spatial and temporal variability, *Prog. Oceanogr.*, *63*, 57–98.

Balch, W. M., D. T. Drapeau, B. C. Bowler, E. S. Booth, L. A. Windecker, and A. Ashe (2008), Space-time variability of carbon standing stocks and fixation rates in the Gulf of Maine, along the GNATS transect between Portland, ME and Yarmouth, NS, *J. Plankton Res.*, *30*(2), 119–139.

Balch, W. M., D. T. Drapeau, B. C. Bowler, and T. Huntington (2012), Step-changes in the physical, chemical and biological characteristics of the Gulf of Maine, as documented by the GNATS time series, *Mar. Ecol.: Prog. Ser.*, *450*, 11–35.

Bauer, J. E., W. J. Cai, P. A. Raymond, T. S. Bianchi, C. S. Hopkinson, and P. A. G. Regnier (2013), The changing carbon cycle of the coastal ocean, *Nature*, *504*(7478), 61–70.

Bigelow, H. B. (1924), Physical oceanography of the Gulf of Maine, *Fish. Bull.*, *40*, 511–1027.

Blough, N. V., O. C. Zafiriou, and J. Bonilla (1993), Optical absorption spectra of waters from the Orinoco River outflow: Terrestrial input of colored organic matter to the Caribbean, *J. Geophys. Res.*, *98*, 2271–2278.

Boysen-Jensen, B. (1914), Studies concerning the organic matter of the sea bottom, *Rep. Danish Biol. Stn.*, *22*, 1–39.

Bricaud, A., A. Morel, and L. Prieur (1981), Absorption by dissolved organic matter of the sea (yellow substance) in the UV and visible domains, *Limnol. Oceanogr.*, *26*(1), 43.

Butman, D., P. A. Raymond, K. Butler, and G. Aiken (2012), Relationships between $\delta^{14}C$ and the molecular quality of dissolved organic carbon in rivers draining to the coast from the conterminous United States, *Global Biogeochem. Cycles*, *26*, GB4014, doi:10.1029/2012GB004361.

Carlson, C. A., H. W. Ducklow, D. A. Hansell, and W. O. Smith Jr. (1998), Organic carbon partitioning during spring phytoplankton blooms in the Ross Sea polynya and the Sargasso Sea, *Limnol. Oceanogr.*, *43*(3), 375–386.

Chen, M. S., S. Wartel, and S. Temmerman (2005), Seasonal variation of floc characteristics on tidal flats, the Scheldt estuary, *Hydrobiologia*, *540*(1–3), 181–195.

Collins, M., et al. (2013), Long-term climate change: Projections, commitments and irreversibility, in *Climate Change 2013: The Physical Science Basis. Contribution of Working Group I to the Fifth Assessment Report of the Intergovernmental Panel on Climate Change*, edited by T. F. Stocker et al., pp. 1029–1136, Cambridge Univ. Press, Cambridge, U. K., and New York.

Cronan, C. S., J. T. Piampiano, and H. H. Patterson (1999), Influence of land use and hydrology on exports of carbon and nitroge in a Maine River Basin, *J. Environ. Qual.*, *28*, 953–961.

Dall'Olmo, G., T. K. Westberry, M. Beherenfeld, E. Boss, and W. H. Slade (2009), Significant contribution of large particles to optical backscattering in the open ocean, *Biogeosciences*, *6*, 947–967.

DeGrandpre, M. D., A. Vodacek, R. K. Nelson, E. J. Bruce, and N. V. Blough (1996), Seasonal seawater optical properties of the U.S. Middle Atlantic Bight, *J. Geophys. Res.*, *101*(C10), 22,727–22,736.

Del Castillo, C. E., P. G. Coble, R. N. Conmy, F. E. Muller-Karger, L. Vanderbloemen, and G. A. Vargo (2001), Multispectral in situ measurements of organic matter and chlorophyll fluorescence in seawater: Documenting the intrusion of the Mississippi River plume in the West Florida Shelf, *Limnol. Oceanogr.*, *46*(7), 1836–1843.

Del Castillo, C. E., et al. (2013), Pre-Aerosol, Clouds, and ocean Ecosystem (PACE) Mission science definition team report *Rep.*, 274 pp., NASA Headquarters, Washington, D. C.

Del Vecchio, R., and N. V. Blough (2004), On the origin of the optical properties of humic substances, *Environ. Sci. Technol.*, *38*(14), 3885–3891.

Dussart, B. M. (1965), Les differentes categories de plancton, *Hyrobiologia*, *26*, 72–74 (with Erratum).

Ferrari, G. M., M. D. Dowell, S. Grossi, and C. Targa (1996), Relationship between the optical properties of chromophoric dissolved organic matter and total concentration of dissolved organic carbon in the southern Baltic Sea region, *Mar. Chem.*, *55*(3–4), 299–316.

Fichot, C., and R. Benner (2011), A novel method to estimate DOC concentrations from CDOM absorption coefficients in coastal waters, *Geophys. Res. Lett.*, *38*, LO3610, doi:10.1029/2010GL046152.

Fichot, C. G., and R. Benner (2012), The spectral slope coefficient of chromophoric dissolved organic matter (S275–295) as a tracer of terrigenous dissolved organic carbon in river-influenced ocean margins, *Limnol. Oceanogr.*, *57*(5), 1453–1466.

Fichot, C. G., S. Sathyendranath, and W. L. Miller (2008), SeaUV and SeaUVC: Algorithms for the retrieval of UV/Visible diffuse attenuation coefficients from ocean color, *Remote Sens. Environ.*, *112*(4), 1584–1602.

Forel, F. A. (1890), Une nouvelle forme de la gamme de couleur pour l'étude de l'eau des lacs, *Arch. Sci. Phys. Nat./Soc. Phys. Hist. Nat. Geneve*, *6*, 25.

Gardner, W. D., and L. G. Sullivan (1981), Benthic storms: Temporal variability in a deep-ocean nepheloid layer, *Science*, *213*(4505), 329–331.

Gordon, C., C. Cooper, C. A. Senior, H. Banks, J. M. Gregory, T. C. Johns, J. F. B. Mitchell, and R. A. Wood (2000), The simulation of SST, sea ice extents and ocean heat transports in a version of the Hadley Centre coupled model without flux adjustments, *Clim. Dyn.*, *16*(2–3), 147–168.
Green, S. A., and N. V. Blough (1994), Optical absorption and fluorescence properties of chromophoric dissolved organic matter in natural waters, *Limnol. Oceanogr. Methods*, *39*(8), 1903–1916.
Griffith, D. M., and C. L. Alerich (1996), *Forest Statistics for Maine, 1995*, USDA Forest Service, Radnor, Pa.
Hayhoe, K., et al. (2007), Past and future changes in climate and hydrological indicators in the U.S. Northeast, *Clim. Dyn.*, *28*, 381–407.
Hedges, J. I., R. G. Keil, and R. Benner (1997), What happens to terrestrial organic matter in the ocean?, *Org. Geochem.*, *27*(5–6), 195–212.
Helie, J.-F., and C. Hillaire-Marcel (2006), Sources of particulate and dissolved organic carbon in the St Lawrence River: Isotopic approach, *Hydrol. Process.*, *20*(9), 1945–1959.
Hodgkins, G. A., and R. W. Dudley (2005), Changes in the magnitude of annual and monthly streamflows in New England, 1902–2002, *Rep. SIR 2005-5235*, 37 pp., U.S. Geological Survey Scientific Investigations.
Hudon, C., R. Morin, J. Bunch, and R. Harland (1996), Carbon and nutrient output from the Great Whale River (Hudson Bay) and a comparison with other rivers around Quebec, *Can. J. Fish. Aquat. Sci./J. Can. Sci. Halieutiques Aquat.*, *53*(07), 1513–1525.
Huntington, T. G. (2006), Evidence for intensification of the global water cycle: Review and synthesis, *J. Hydrol.*, *319*, 83–95.
Huntington, T. G., and G. R. Aiken (2013), Export of dissolved organic carbon from the Penobscot River basin in north-central Maine, *J. Hydrol.*, *476*, 244–256.
Huntington, T. G., and M. Billmire (2014), Trends in precipitation, runoff, and evapotranspiration for rivers draining to the Gulf of Maine in the United States, *J. Hydrometeorol.*, *15*(2), 726–743.
Kirchman, D. L., Y. Suzuki, C. Garside, and H. W. Ducklow (1991), High turnover rates of dissolved organic carbon during a spring phytoplankton bloom, *Nature*, *352*(6336), 612–614.
Liang, X., E. F. Wood, and D. P. Lettenmaier (1996), Surface soil moisture parameterization of the VIC-2 L model: Evaluation and modifications, *Global Planet. Change*, *13*, 195–206.
Ludwig, W., and J. L. Probst (1996), Predicting the oceanic input of organic carbon by continental erosion, *Global Biochem. Cycles*, *10*(1), 23–41.
Mague, T. H., E. Friberg, D. J. Hughes, and I. Morris (1980), Extracellular release of carbon by marine phytoplankton: A physiological approach, *Limnol. Oceanogr.*, *25*, 262–279.
Mannino, A., M. E. Russ, and S. B. Hooker (2008), Algorithm development and validation for satellite-derived distributions of DOC and CDOM in the U.S. Middle Atlantic Bight, *J. Geophys. Res.*, *113*, C07051, doi:10.1029/2007JC004493.
Mannino, A., M. G. Novak, S. B. Hooker, K. Hyde, and D. Aurin (2014), Algorithm development and validation of CDOM properties for estuarine and continental shelf waters along the northeastern U.S. coast, *Remote Sens. Environ.*, *152*, 576–602.
Meade, R. H., and K. O. Emery (1971), Sea level as affected by river runoff, Eastern United States, *Science*, *173*, 425–428.
Mobley, C. D. (1994), *Light and Water: Radiative Transfer in Natural Waters*, 592 pp., Academic Press, New York.
Morel, A., and Y. Ahn (1991), Optics of heterotrophic nanoflagellates and ciliates: A tentative assessment of their scattering role in oceanic waters compared to those of bacterial and algal cells, *J. Mar. Res.*, *49*, 177–202.
Nakićenović, N. (2000), Special report on emissions scenarios: A special report of Working Group III of the Intergovernmental Panel on Climate Change *Rep.*, Pacific Northwest National Laboratory (PNNL) Environmental Molecular Sciences Laboratory (EMSL), Richland, Wash.
Opsahl, S., and R. Benner (1998), Photochemical reactivity of dissolved lignin in river and ocean waters, *Limnol. Oceanogr.*, *43*, 1297–1304.
Orellana, M. V., T. W. Petersen, A. H. Diercks, S. Donohoe, P. Verdugo, and G. van den Engh (2007), Marine microgels: Optical and proteomic fingerprints, *Mar. Chem.*, *105*(3–4), 229–239.
Pak, H., J. Ronald, V. Zaneveld, and J. Kitchen (1980), Intermediate nepheloid layers observed off Oregon and Washington, *J. Geophys. Res.*, *85*(C11), 6697–6708.
Pettigrew, N. R., D. W. Townsend, H. Xue, J. P. Wallinga, P. J. Brickley, and R. D. Hetland (1998), Observations of the Eastern Maine Coastal Current and its offshore extensions in 1994, *J. Geophys. Res.*, *103*(C13), 30,623–30,639.
Pilskaln, C. H., K. Hayashi, B. A. Keafer, D. M. Anderson, and D. J. McGillicuddy (2014), Benthic nepheloid layers in the Gulf of Maine and Alexandrium cyst inventories, *Deep Sea Res., Part II*, *103*, 55–65.
Pocklington, R., and F. C. Tan (1987), Seasonal and annual variations in the organic matter contributed by the St. Lawrence River to the Gulf of St. Lawrence, *Geochim. Cosmochim. Acta*, *51*, 2579–2586.
Pope, V. D., M. L. Gallani, P. R. Rowntree, and R. A. Stratton (2000), The impact of new physical parameterizations in the Hadley Centre climate model—HadCM3, *Clim. Dyn.*, *16*, 123–146.
Power, S., F. Delage, R. Colman, and A. Moise (2012), Consensus on twenty-first century rainfall projections in climate models more widespread than previously thought, *J. Clim.*, *25*, 3792–3809.
Ramp, S. R., R. J. Schlitz, and W. R. Wright (1985), The deep flow through the Northeast Channel, Gulf of Maine, *J. Phys. Oceanogr.*, *15*, 1790–1808.
Roesler, C. S., and M. J. Perry (1989), Modeling in situ phytoplankton absorption from total absorption spectra in productive inland marine waters, *Limnol. Oceanogr.*, *34*(8), 1510–1523.
Roesler, C. S., A. H. Barnard, G. Aiken, T. Huntington, W. M. Balch, and H. Xue (2006), Using optical proxies for biogeochemical properties to study land coverage and terrestrial inputs of organic carbon into coastal waters from the Penobscot Watershed to the Gulf of Maine, paper presented at Proceeding of Ocean Optics XVIII, Montreal, Quebec, 9–13 October, 2006.
Runkel, R. L., C. G. Crawford, and T. A. Cohn (2004), *Load Estimator (LOADEST): A FORTRAN Program for Estimating Constituent Loads in Streams and Rivers*, 68 pp., U.S. Geol. Surv., Denver, Colo.
Seager, R., N. Naik, and L. Vogel (2012), Does global warming cause intensified interannual hydroclimate variability?, *J. Clim.*, *25*(9), 3355–3372.
Siegel, D. A., S. Maritorena, N. B. Nelson, D. A. Hansell, and M. Lorenzi-Kayser (2002), Global distribution and dynamics of colored dissolved and detrital organic materials, *J. Geophys. Res.*, *107*(C12), 3228, doi:10.1029/2001JC000965.
Siegel, D. A., S. Maritorena, N. B. Nelson, M. J. Behrenfeld, and C. R. McClain (2005), Colored dissolved organic matter and its influence on the satellite-based characterization of the ocean biosphere, *Geophys. Res. Lett.*, *32*, L20605, doi:10.1029/2005GL024310.
Siegenthaler, U., and J. L. Sarmiento (1993), Atmospheric carbon dioxide and the ocean, *Nature*, *365*(6442), 119–125.
Smith, P. C. (1983), The mean and seasonal circulation off southwest Nova Scotia, *J. Phys. Oceanogr.*, *13*, 1034–1054.
Smith, P. C., R. W. Houghton, R. G. Fairbanks, and D. G. Mountain (2001), Interannual variability of boundary fluxes and water mass properties in the Gulf of Maine and on Georges Bank: 1993–1997, *Deep Sea Res., Part II*, *48*(1), 37–70.
Spinrad, R. W., J. R. V. Zaneveld, and J. C. Kitchen (1983), A study of the optical characteristics of the suspended particles in the benthic nepheloid layer of the Scotian Rise, *J. Geophys. Res.*, *88*(C12), 7641–7645.
Stedmon, C. A., and S. Markager (2001), The optics of chromophoric dissolved organic matter (CDOM) in the Greenland Sea: An algorithm for differentiation between marine and terrestrially derived organic matter, *Limnol. Oceanogr.*, *46*(8), 2087–2093.

Stramski, D., and D. A. Kiefer (1991), Light scattering by microorganisms in the open ocean, *Prog. Oceanogr.*, *28*(4), 343–383.
Sun, F., M. L. Roderick, and G. D. C. L. Farquhar (2012), Changes in the variability of global land precipitation, *Geophys. Res. Lett.*, *39*, L19402, doi:10.1029/2012GL053369.
Sutcliffe, W. H., Jr., R. H. Loucks, and K. F. Drinkwater (1976), Coastal circulation and physical oceanography of the Scotian Shelf and Gulf of Maine, *J. Fish. Res. Board Can.*, *33*, 98–115.
Thibeault, J., and A. Seth (2014), Changing climate extremes in the Northeast United States: Observations and projections from CMIP5, *Clim. Change*, *127*(2), 273–287.
Thompson, C. (2010), The Gulf of Maine in context: State of the Gulf of Maine report *Rep.*, 56 pp, Gulf of Maine Council on the Environment.
Tian, H., Q. Yang, R. G. Najjar, W. Ren, M. A. M. Friedrichs, C. S. Hopkinson, and S. Pan (2015), Anthropogenic and climatic influences on carbon fluxes from eastern North America to the Atlantic Ocean: A process-based modeling study, *J. Geophys. Res. Biogeosci.*, *120*, 752–772, doi:10.1002/2014JG002760.
Townsend, D. W. (1998), Sources and cycling of nitrogen in the Gulf of Maine, *J. Mar. Syst.*, *16*, 283–295.
Tranvik, L. J., and M. Jansson (2002), Terrestrial export of dissolved organic carbon, *Nature*, *415*, 861–863.
Ule, W. (1892), Die Bestimmung der Wasserfarbe in den Seen, in *Kleinere Mittheilungen aus Justus Perthes' Geographischer Anstalt uber wichtige neue Erforschungen auf dem Gesammtgebiete der Geographie*, edited by A. Petermanns and J. Perthes, pp. 70–71, Justus Perthes, Gotha.
Vaillancourt, R. D., J. Marra, L. Prieto, R. W. Houghton, B. Hales, and D. Hebert (2005), Light absorption and scattering by particles and CDOM at the New England shelfbreak front, *Geochem. Geophys. Geosyst.*, *6*, Q11003, doi:10.1029/2005GC000999.
Vodacek, A., N. V. Blough, M. D. DeGrandpre, E. T. Peltzer, and R. K. Nelson (1997), Seasonal variation of CDOM and DOC in the Middle Atlantic Bight: Terrestrial inputs and photooxidation, *Limnol. Oceanogr.*, *42*(4), 674–686.
Waksman, S. A. (1933), On the distribution of organic matter in the sea bottom and the nature and origin of marine humis, *Soil Sci.*, *36*, 125–147.
Walter, M. T., D. S. Wilks, J.-Y. Parlange, and R. L. Schneider (2004), Increasing evapotranspiration from the conterminous United States, *J. Hydrometeorol.*, *5*(3), 405–408.
Weishaar, J. L., G. R. Aiken, B. A. Bergamaschi, M. S. Fram, and R. Fujii (2003), Evaluation of specific ultra-violet absorbance as an indicator of the chemical composition and reactivity of dissolved organic carbon, *Environ. Sci. Technol.*, *37*, 4702–4708.
Werdell, P. J., et al. (2013), Generalized ocean color inversion model for retrieving marine inherent optical properties, *Appl. Opt.*, *52*(10), 2019–2037.
Wernand, M. R., and H. J. Van Der Woerd (2010), Spectral analysis of the Forel-Ule ocean colour comparator scale, *J. Eur. Opt. Soc.-Rapid Publ.*, *5*, 10014S.
Wetzel, R. G. (1975), Organic carbon cycle and detritus, 743 pp., W. B. Saunders Co., Philadelphia, Pa.
Wolanski, E., and R. J. Gibbs (1995), Flocculation of suspended sediment in the Fly River Estuary, Papua New Guinea, *J. Coastal Res.*, *11*(3), 754–762.
Wyszecki, G., and W. S. Stiles (1982), *Color Science: Concepts and Methods, Quantitative Data and Formulae*, 2nd ed., John Wiley, New York.
Yentsch, C. S., and D. A. Phinney (1997), Yellow substances in the coastal waters of the Gulf of Maine: Implications for ocean color algorithms, paper presented at SPIE, SPIE, Halifax, Nova Scotia, Canada, 22 Oct. 1996.
Yoon, B., and P. A. Raymond (2012), Dissolved organic matter export from a forested watershed during Hurricane Irene, *Geophys. Res. Lett.*, *39*. L18402, doi:10.1029/2012GL052785.
Zhang, X., and D. J. Gray (2015), Backscattering by very small particles in coastal waters, *J. Geophys. Res. Oceans*, *120*, 6914–6926, doi:10.1002/2015JC010936.